Statistical rate theory for the HO+O⇔HO 2 ⇔H+O 2 reaction system: SACM/CT calculations between 0 and 5000 K

L. B. Harding, A. I. Maergoiz, J. Troe, and V. G. Ushakov

Citation: The Journal of Chemical Physics **113**, 11019 (2000); doi: 10.1063/1.1314374
View online: http://dx.doi.org/10.1063/1.1314374
View Table of Contents: http://scitation.aip.org/content/aip/journal/jcp/113/24?ver=pdfcov
Published by the AIP Publishing

Statistical rate theory for the HO+O⇔HO_2⇔H+O_2 reaction system: SACM/CT calculations between 0 and 5000 K

L. B. Harding,[a] A. I. Maergoiz,[b] J. Troe,[c] and V. G. Ushakov[d]
Institut für Physikalische Chemie, Universität Göttingen, Tammannstrasse 6, D-37077 Göttingen, Germany

(Received 31 May 2000; accepted 10 August 2000)

The potential energy surface of the HO+O⇔HO_2⇔H+O_2 reaction system is characterized by *ab initio* calculations. The complex-forming bimolecular reaction is then treated by statistical rate theory, using statistical adiabatic channel and classical trajectory calculations for the HO+O⇔HO_2 and HO_2⇔H+O_2 association/dissociation processes. Specific rate constants $k(E,J)$ of both reactions as well as thermal rate constants are calculated over wide ranges of conditions. Open shell quantum effects are important up to room temperature. The good agreement with experimental results suggests that the *ab initio* potential is of sufficient accuracy. There is no evidence for non-statistical effects or for a significant contribution from electronically excited states. The comparison with rate data for the H+O_2→HO+O reaction, because of the remaining uncertainty in the heat of formation of HO, is somewhat inconclusive. Apart from this problem, the calculated rate constants appear reliable between 0 and 5000 K. © *2000 American Institute of Physics.* [S0021-9606(00)70142-5]

I. INTRODUCTION

The elementary bimolecular gas phase reaction

$$(k_1) \quad \mathrm{H+O_2 \rightarrow HO+O} \tag{1.1}$$

''remains perhaps the most fascinating example of how the most detailed microscopic dynamical behavior can have a major impact on even the most macroscopic of combustion phenomena,'' as J. A. Miller states in his review of theory and modeling in combustion chemistry.[1] Because of its great practical importance, the reaction is among the most intensely studied elementary gas phase reactions. However, in spite of considerable effort both on the experimental and on the theoretical side, many questions about this reaction are still open and call for new and more detailed work. The present article continues the investigations on the theoretical side, being however in close relation to experimental applications. An exhaustive review of previous work cannot possibly be given at this place, but the cited references should provide sufficient links to earlier publications.

It appears obligatory to always consider reaction (1.1) together with its reverse reaction

$$(k_2) \quad \mathrm{HO+O \rightarrow H+O_2}, \tag{1.2}$$

as k_1 and k_2 are connected by the equilibrium constant,

$$K_{\mathrm{eq}} = k_1/k_2. \tag{1.3}$$

The combined measurements of k_1 and k_2 now cover the temperature range 160–5300 K, extensions down into the 10 K range are becoming possible.[2] The measured values of k_2 between 160 and 500 K (see Refs. 3–6) vary within about ±15%. The scatter of the more numerous measurements of k_1 between about 700 and 5300 K (see Refs. 7–20; for reviews of earlier work, see Refs. 21–23) is somewhat larger, being about ±25% at 2000 K. In combining k_1 and k_2 through the equilibrium constant, Eq. (1.3), the remaining uncertainty in K_{eq}, introduced by the still fairly large uncertainty in the enthalpy of formation of HO [being about ±2 kJ mol^{-1} (Refs. 24–26)], should be kept in mind. One should also take into account that vibrational disequilibrium may have[27] (or not have[28]) been present under some of the experimental conditions.

Any interpretation of k_1 and k_2 has also to account for measurements of the rate constant of the recombination reaction

$$(k_4) \quad \mathrm{H+O_2(+M) \rightarrow HO_2(+M)}, \tag{1.4}$$

in its falloff range up to the high pressure limit[29] and for information about vibrational deactivation processes such as

$$\mathrm{H+O_2}(v) \rightarrow \mathrm{H+O_2}(v') \tag{1.5}$$

or O+OH(v)→O+OH(v') which take place on the same potential energy surface as reactions (1.1), (1.2), and (1.4). Extensive measurements of inelastic and reactive cross sections are available in addition (see, e.g., Refs. 30–40). The derived cross sections should be interpreted consistent with the thermal rate constants. One should, however, note that a series of earlier results recently have been shown to be considerably in error,[40] such that previous conclusions should be used with caution.

On the theoretical side, numerous methods have been applied to the reaction system. Among the used potential energy surfaces are those by Melius and Blint,[41] by Varandas and co-workers,[42] and by Kendrick and Pack.[43] The most

[a]Present address: Chemistry Division, Argonne National Laboratory, 9700 South Cass Avenue, Argonne, Illinois 60439.
[b]On leave from N. N. Semenov Institute of Chemical Physics, Russian Academy of Sciences, 117977 Moscow, Russia.
[c]Author to whom correspondence should be addressed.
[d]Present address: Institute of Problems of Chemical Physics, Russian Academy of Sciences, 142432 Chernogolovka, Russia.

frequently used DMBE IV global surface[42] unfortunately differs considerably from *ab initio* results. In our previous work on reaction (1.4),[44] we noticed marked differences in a range of H–OO distances which are of central importance for the kinetics of reaction (1.4), the same being true for the earlier Melius–Blint surface. Marked differences between the DMBE IV surface and the *ab initio* calculations by Walch and co-workers[45–47] were also noticed in Ref. 48 for a range of HO–O distances which govern the kinetics of reactions (1.1) and (1.2). At the same time, a comparison of our earlier *ab initio* calculations for reaction (1.4) (Ref. 44) with the results from Ref. 45 indicated that highest level *ab initio* calculations are required to obtain the necessary accuracy at intermediate H–OO and HO–O distances. In the present work, we extend our earlier *ab initio* calculations from the H–OO to the HO–O side of the HO_2 reaction system. While the complete characterization of all of the electronic states of HO_2 correlating with $O(^3P_{2,1,0})$ and $HO(^2\Pi_{3/2,1/2})$ (Ref. 49) remains a challenging task for the future, in the present work we have concentrated on the two lowest electronic states of HO_2 correlating with $O(^3P_2)$ and $HO(^2\Pi_{3/2})$. The question of a participation of the upper of these two potentials,[50] which does not correlate with electronic ground state HO_2, needs further investigations, see below. Besides full empirical or *ab initio* characterization of the potential, such as employed in full classical trajectory or quantum scattering calculations, empirical models of parts of the potential, such as required for statistical treatments, have also been designed[50,51] (based in part on *ab initio* calculations from Ref. 52; long-range representations of the potential have been used as well[53]). Under suitable conditions, these partial characterizations of the potential may surprisingly well capture the essential features of the reaction dynamics, see below.

The long history of calculating the rate of reaction (1) includes a variety of full quasiclassical trajectory (QCT) calculations (see, e.g., Refs. 42, 54–60), variational transition state theory (VTST) on the canonical and microcanonical level (see, e.g., Refs. 48, 54, 61–65), simplified statistical adiabatic channel (SACM) treatments,[29,50] and 3D-quantum scattering calculations.[66–72] Sometimes, marked disagreement between experiment and theory was found. In some instances agreement with the experiments later on was also identified as fortuitous and caused by cancelling of errors.

The merits of the various approaches cannot be discussed at this place. Instead a number of open questions are considered, to which the present work may provide some answers.

(i) In previous work, frequently the DMBE IV potential was used, sometimes leading to unacceptable disagreement with the experiments, sometimes to agreement (see e.g., Ref. 48). A disagreement sometimes today can be attributed to the imperfections of the DMBE IV surface. We investigate how far our new *ab initio* potential, combined with a detailed statistical theory, can reproduce experimental results for reactions (1.1), (1.2), and (1.4) over wide ranges of conditions.

(ii) The question of ''non-RRKM'' effects in reaction (1.1) has been raised[1,42,54,55] and analyzed by comparing QCT and classical microcanonical VTST calculations.[54] Marked ''non-RRKM'' behavior was observed in the form of recrossing trajectories, originating from HO+O and leading back to HO+O in spite of the high exothermicity of the exit to $H+O_2$. We approach the question of ''nonstatistical'' behavior (instead of the less appropriate term ''non-RRKM'') by replacing microcanonical VTST by a more detailed statistical theory. We apply our recent version of the statistical theory which combines rigorous adiabatic channel calculations with classical trajectory calculations for capture processes (we call this approach SACM/CT; for other recent applications, see, e.g., Refs. 44, 73–75). We try to trace the origin of the mentioned ''non-RRKM'' effects. Our present treatment does not provide evidence for nonstatistical effects.

(iii) In analyzing nonstatistical effects, Miller and Garrett,[1,54] discussed the possibility of calculational artifacts caused by the difficulty of handling zero point energy of high frequency vibrations in QCT calculations.[76] In the present work, trajectories were only followed during the capture part of the dynamics, employing rigid rotor diatomics at their equilibrium bond lengths. The zero point energy problem thus could essentially be avoided. We suggest that the observed nonstatistical effects are an indirect consequence of the fully classical QCT treatment.

(iv) The SACM/CT treatment allows us to properly account for angular momentum conservation. This is particularly important in the present system with different reduced moments of inertia on the HO–O and $H–O_2$ side of the potential. Simplified treatments such as the ''*J*-shifting'' method, used for quantum scattering calculations,[67] may have been oversimplified. On the other hand, the complete characterization of the *J*-dependencies in quantum scattering calculations requires large effort and is becoming available only slowly.[71,72] The present statistical treatment provides a much more economic and apparently sufficiently accurate access to *J*-effects. For O+OH capture at moderately low temperatures, also spin and electronic angular momentum of OH and O have to be included in the treatment. Rigorous SACM treatments have been demonstrated[77] to be able to account for these refinements.

(v) The rate constants of the bimolecular reactions (1.1) and (1.2) as well as for the high pressure limit of reaction (1.4) in statistical theory do not include specific rate constants $k(E,J)$ of HO_2 dissociation but only numbers of open channels $W(E,J)$ for the dissociation/association of HO_2 (subscript ''*a*'' for $HO_2^* \Leftrightarrow HO+O$, subscript ''*b*'' for $HO_2^* \Leftrightarrow H+O_2$). Considering reaction only in the ground electronic state of HO_2, for HO+O capture

$$(k_6) \quad HO+O \rightarrow HO_2, \tag{1.6}$$

one has a rate constant

$$k_6 = \frac{kT}{h}\left(\frac{h^2}{2\pi\mu_a kT}\right)^{3/2} \frac{Q_{el}(HO_2)}{Q_{el}(HO)Q_{el}(O)} \frac{1}{Q_{vibrot}(HO)} \times \sum_{J=0}^{\infty} (2J+1) \int_{E_{0a}}^{\infty} W_a(E,J) \exp\left(-\frac{E-E_{0a}}{kT}\right) \frac{dE}{kT}, \tag{1.7}$$

with the rovibrational partition function Q_{vibrot} the electronic partition functions Q_{el} and the reduced mass μ_a of the HO+O collision pair. E_{0a} corresponds to the energy of $\text{HO}(^2\Pi_{3/2})+\text{O}(^3P_2)$ in the rovibrational ground state of HO. Likewise, for the high pressure limit of reaction (1.4), k_4 is given by

$$k_4=\frac{kT}{h}\left(\frac{h^2}{2\pi\mu_b kT}\right)^{3/2}\frac{Q_{\text{el}}(\text{HO}_2)}{Q_{\text{el}}(\text{H})Q_{\text{el}}(\text{O}_2)}\frac{1}{Q_{\text{vibrot}}(\text{O}_2)}\times\sum_{J=0}^{\infty}(2J+1)\int_{E_{0b}}^{\infty}W_b(E,J)\exp\left(-\frac{E-E_{0b}}{kT}\right)\frac{dE}{kT}, \tag{1.8}$$

μ_b being the reduced mass of the H+O$_2$ collision pair and E_{0b} is the energy of the rovibrational ground state of O$_2$. Using the same nomenclature, k_2 is given by

$$k_2=\frac{kT}{h}\left(\frac{h^2}{2\pi\mu_a kT}\right)^{3/2}\frac{Q_{\text{el}}(\text{HO}_2)}{Q_{\text{el}}(\text{HO})Q_{\text{el}}(\text{O})}\frac{1}{Q_{\text{vibrot}}(\text{HO})}\times\sum_{J=0}^{\infty}(2J+1)\int_{E_{0a}}^{\infty}W_a(E,J)\times\left[\frac{W_b(E,J)}{W_a(E,J)+W_b(E,J)}\right]\exp\left(-\frac{E-E_{0a}}{kT}\right)\frac{dE}{kT}. \tag{1.9}$$

k_1 is linked to k_2 through the equilibrium constant, Eq. (1.3), i.e., it is given by

$$k_1=\frac{kT}{h}\left(\frac{h^2}{2\pi\mu_b kT}\right)^{3/2}\frac{Q_{\text{el}}(\text{HO}_2)}{Q_{\text{el}}(\text{H})Q_{\text{el}}(\text{O}_2)}\frac{1}{Q_{\text{vibrot}}(\text{O}_2)}\times\sum_{J=0}^{\infty}(2J+1)\int_{E_{0b}}^{\infty}W_b(E,J)\times\left[\frac{W_a(E,J)}{W_a(E,J)+W_b(E,J)}\right]\exp\left(-\frac{E-E_{0b}}{kT}\right)\frac{dE}{kT}. \tag{1.10}$$

Using the statistical relationship

$$k(E,J)=\frac{W(E,J)}{h\rho(E,J)}, \tag{1.11}$$

with the rovibrational density of states $\rho(E,J)$ of HO$_2$, the expressions in brackets in Eqs. (1.9) and (1.10) can also be expressed in terms of ratios of specific rate constants $k(E,J)$. Although not being required for the evaluation of Eqs. (1.7)–(1.10), it appears useful also to calculate $k_a(E,J)$ and $k_b(E,J)$. $k_b(E,J)$, for instance, is required for the detailed calculation of falloff curves for reaction (1.4) (including rotational effects, such as described in Ref. 78). In addition, a comparison is possible with the wave packet calculations of HO$_2$ dissociation rate constants $k(E,J=0)$ from Refs. 69 and 70. The comparison with simplified SACM results, apart from pronounced lifetime fluctuations, on average led to good agreement. This does not prove that reaction (1.1) as a whole behaves statistically without ''non-RRKM'' effects, but it provides some evidence in this direction. Nevertheless, it should be emphasized that the explicit calculation of the rovibrational anharmonic densities of states $\rho(E,J)$ of HO$_2$ is not without problems. Employing the empirical local-mode method from Ref. 79, large fluctuations and irregularities in $\rho(E,J)$ arise. These are even more pronounced than observed in our recent work on NO$_2$ dissociation.[75] However, a comparison of the derived values of $k(E,J=0)$ with the wave packet calculations from Ref. 69 on average nevertheless can be made.

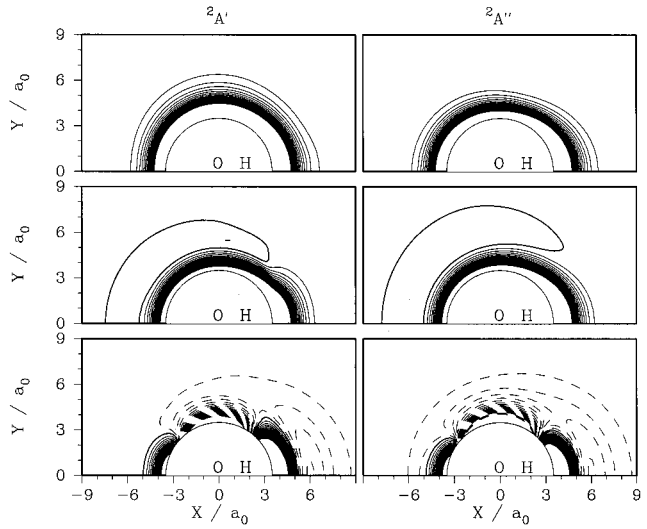

FIG. 1. Equipotential contours for the six lowest electronic states of the HO+O system. The HO bond length is fixed at $1.85a_0$. The contour increment is 1.0 kcal/mol. Solid contours denote regions with energies above that of reactants, dashed contours denote attractive regions, see also Fig. 4.

II. *AB INITIO* CALCULATIONS AND REPRESENTATION OF THE POTENTIAL

The *ab initio* calculations of the present work, like those for the H+O$_2$ side of the potential energy surface described in Ref. 44, use the augmented, correlation-consistent, polarized triple zeta (aug-cc-pvtz) basis set of Dunning[80–82] $(5s,4p,3d,2f/4s,3p,2d)$. The calculations are all of the multireference configuration interaction (MR-CI) variety, employing a five orbital–seven electron, complete active space (CAS) reference wave function. The five active orbitals consist of the oxygen atom, p orbitals and the HO, p orbitals. The orbitals were optimized in a state-averaged MCSCF calculation in which the six doublet states correlating with the $\text{HO}(^2P)+\text{O}(^3P)$ limit were all weighted equally. With these orbitals, MR-CI calculations were carried out to obtain the energies of the six individual states. In order to estimate the importance of higher-order correlations (beyond single and double excitations), a multireference Davidson correction was also applied.[83] All calculations were carried out using the MOLPRO program package.[84,85]

We illustrate in Fig. 1 the change of the anisotropy of the $^2A''$ and $^2A'$ *ab initio* potential energy surfaces with increasing interfragment distance. For the lowest $^2A''$ and $^2A'$ surfaces we find a shallow potential minimum in the linear OH–O configuration as a consequence of the sign of the dipole–quadrupole interaction. For the higher surfaces, the quadruple moment of the O atom is oriented in such a way as to make this interaction repulsive. The much deeper mini-

TABLE I. Stationary points on the CAS+1+2+QC/aug-cc-pvtz, $1\,^2A'$ and $1\,^2A''$ surfaces.

R_{OH}/a_0	R_{OO}/a_0	OOH angle	V/kcal mol^{-1}	ω/cm^{-1}
O+OH				
1.84	⋯	⋯	0.0	3743
O–OH	($^2A'$)			
1.84	5.93	0.0	−2.07	3722,249,249
1.84	5.45	66.4	−0.69	3739,190,309*i*
1.83	2.66	101.4	−43.32	3755,1234,943
O–OH	($^2A''$)			
1.84	5.93	0.0	−2.07	3722,220,220
1.84	5.46	45.6	−1.46	3742,189,187*i*
1.84	2.54	103.9	−63.73	3688,1430,1115

mum of the O–OH valence structure in the almost T-shaped configuration is found at shorter distances. Note that only the lowest $^2A''$ and lowest $^2A'$ are predicted to be reactive.

Minimum energy paths (MEP) were traced in two coordinate systems, bond coordinates (as a function of R_{O-OH}), and Jacobi coordinates (as a function of the distance, r, between the O atom and the HO center-of-mass). In the Jacobi coordinate system, we denote the angle γ to be the angle between the O atom, the HO center-of-mass and the hydrogen atom. For both paths, the spectator HO distance was kept fixed at 1.85 a_0. Bend force constants were evaluated along both MEP. The frequencies were then obtained by diagonalizing the mass-weighted force constant matrix as described previously.[86] Three stationary points were found on each of the two lowest surfaces, the reactant, OH+O, the covalently bonded product, HO_2, and a long-range, linear, hydrogen-bonded or dipole–quadrupole-bonded intermediate. The geometries, energies and harmonic frequencies for these stationary points are listed in Table I. The linear minima on the $^2A''$ and $^2A'$ surfaces are degenerate, both being components of a $^2\Pi$ state. The bend frequencies of these two states, however, are nondegenerate. Although the spectator HO bond is kept fixed in the MEP calculations, it was optimized for each of the minima. From the results in Table I it can be seen that the variations in this coordinate are inconsequential.

The results of the MEP calculations are shown graphically in Figs. 2 and 3 and tabulated in Tables II–V. Figure 2 illustrates the *ab initio* results for the MEP energies, Fig. 3 shows the MEP bending frequencies. For a short distance, near $r=5.3a_0$, the calculations predict a double-minimum in the bend potential. As a consequence of this there is a discontinuous jump in the geometry of the MEP from nearly T-shaped to linear.

The calculated, equilibrium, dissociation energy of $HO_2(X\,^2A'')$ is 63.7 kcal mol^{-1}. Including zero point energies gives a ΔH_0(HO–O) of 60.6 kcal mol^{-1}, 3.7 kcal mol^{-1} smaller than the experimental value[24–26,87] of 64.3 kcal mol^{-1}. The energy difference between the $X\,^2A''$ and $A\,^2A'$ states of HO_2 is in excellent agreement with experiment[88,89] (20.0 vs 20.1 kcal mol^{-1}, respectively). As in previous studies,[44,90] we scale the MEP energy to reproduce the experimental values. The MEP angles and frequencies are left unchanged. One should, however, keep in mind that the uncertainty in the experimental dissociation energy is still about ± 0.8 kcal mol^{-1},[87] see below.

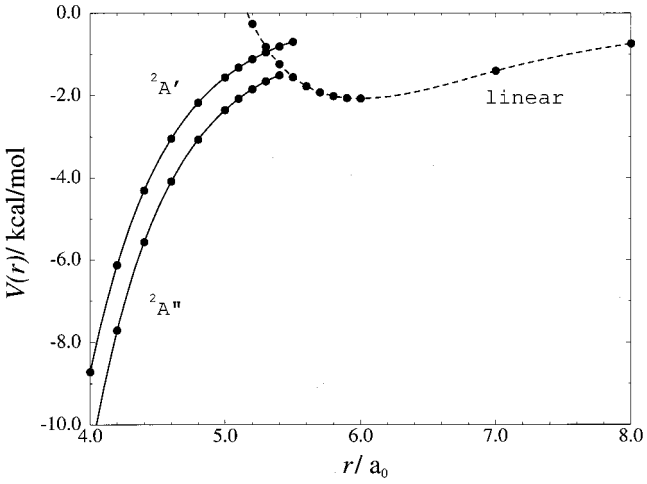

FIG. 2. MEP energies $V(r)$ as a function of r. The dotted line is a collinearly constrained MEP, the solid lines are noncollinear paths.

The present *ab initio* calculations are quite similar to those from Refs. 45–47. There are three differences between the present calculations and those of Refs. 45–47.

(i) The present calculations were all done using an aug-pvtz basis set while the earlier calculations were done using both pvtz (primarily) and aug-pvtz basis sets; (ii) the present CASSCF calculations used a 5 orbital active space while the previous calculations used both 4 orbital (primarily) and 5 orbital active spaces; and (iii) the present calculations used a state-averaged CASSCF calculation while the previous calculations optimized for the $X\,^2A''$ state. The present calculations then are designed to yield an accurate description of the long-range, OH–O, interaction where both diffuse functions and interactions between multiple, nearly degenerate, surfaces are important.

Obviously it is not trivial to represent the *ab initio* results in analytical form. One cannot expect to be able to

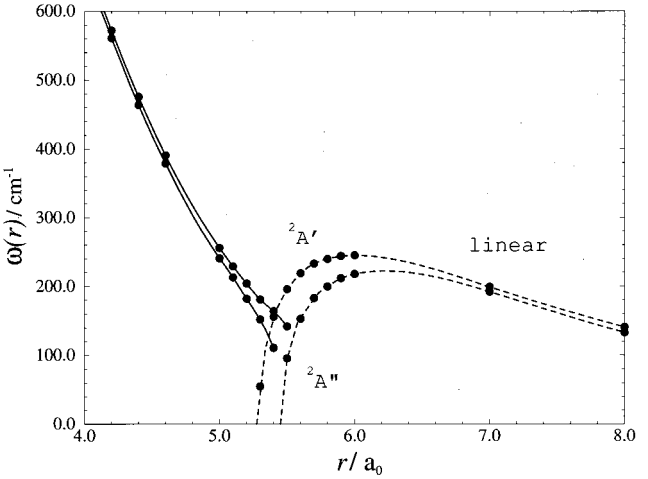

FIG. 3. MEP bend harmonic frequencies $\omega(r)$ as a function of r. The dotted lines are from a collinearly constrained MEP, the solid lines are noncollinear paths.

TABLE II. CAS+1+2+QC/aug-cc-pvtz, minimum energy path for the reaction HO+O→HO$_2$($X\,^2A''$) in bond coordinates.

R_{OC}/a_0	OOH angle	$V(R_{OO})$/kcal mol^{-1}	ω(bend)/cm^{-1}
15.0	0.0	−0.04	25
12.0	0.0	−0.10	39
10.0	0.0	−0.25	66
9.0	0.0	−0.42	92
8.0	0.0	−0.75	133
7.0	0.0	−1.41	192
6.0	0.0	−2.08	218
5.5	0.0	−1.55	96
5.0	81.1	−2.35	241
4.6	84.1	−4.09	379
4.4	85.0	−5.57	464
4.2	85.9	−7.71	561
4.0	86.8	−10.81	666
3.8	87.8	−15.24	778
3.6	89.1	−21.30	887
3.4	90.7	−29.12	994
3.2	92.9	−38.42	1091
3.0	95.6	−48.55	1189
2.8	98.9	−57.62	1290

employ a similarly simple anisotropy function as designed for the H–OO side of the potential.[44] Nevertheless, we found a surprisingly simple representation of the potential for the HO–O side. In Jacobi coordinates, r and γ, this is of the form

$$V(r,\gamma)=V(r)+a_2(r)x^2+a_3(r)x^3+a_4(r)x^4 \tag{2.1}$$

with

$$x=\cos\gamma-\cos\gamma_0(r). \tag{2.2}$$

$V(r)$ is the scaled MEP potential energy and $\gamma_0(r)$ is the equilibrium angle of the MEP. Expressing r in atomic units a_0 and $V(r)$ in kcal mol^{-1}, we interpolate $\gamma_0(r)$ in the form

$$\cos\gamma_0(r)=0.123-1.881r\exp(-0.968r) \tag{2.3}$$

TABLE III. CAS+1+2+QC/aug-cc-pvtz, minimum energy path for the reaction HO+O→HO$_2$($^2A'$) in bond coordinates.

R_{OC}/a_0	OOH angle	$V(R_{OO})$/kcal mol^{-1}	ω(bend)/cm^{-1}
15.0	0.0	−0.04	25
12.0	0.0	−0.10	42
10.0	0.0	−0.25	70
9.0	0.0	−0.42	96
8.0	0.0	−0.75	141
7.0	0.0	−1.41	199
6.0	0.0	−2.08	245
5.5	0.0	−1.55	196
5.5	94.0	−0.70	142
5.0	90.2	−1.56	256
4.6	88.8	−3.05	391
4.4	88.6	−4.31	476
4.2	88.6	−6.13	572
4.0	88.9	−8.72	678
3.8	89.5	−12.32	788
3.6	90.4	−17.10	897
3.4	91.7	−23.16	1001
3.2	93.4	−29.99	1089
3.0	95.7	−36.76	1162
2.8	98.7	−41.93	1212

TABLE IV. CAS+1+2+QC/aug-cc-pvtz, minimum energy path for the reaction HO+O→HO$_2$($X\,^2A''$) in Jacobi coordinates.

r/a_0	γ	$V(r)$/kcal mol^{-1}	ω(bend)/cm^{-1}
15.0	0.0	−0.03	22
12.0	0.0	−0.10	37
10.0	0.0	−0.23	66
9.0	0.0	−0.39	89
8.0	0.0	−0.70	125
7.0	0.0	−1.32	182
6.5	0.0	−1.74	210
6.0	0.0	−2.06	220
5.8	0.0	−2.07	213
5.6	0.0	−1.80	173
5.5	0.0	−1.65	121
5.4	0.0	−1.44	72
5.2	0.0	−0.72	189i
5.0	0.0	+0.39	333i
5.2	83.9	−1.81	166
5.0	86.7	−2.32	227
4.8	88.1	−3.03	292
4.6	89.1	−4.05	363
4.4	90.0	−5.53	449
4.2	90.9	−7.67	547
4.0	91.9	−10.79	652
3.8	93.2	−15.26	761
3.6	94.7	−21.42	872
3.4	96.4	−29.41	979
3.2	98.6	−39.10	1077
3.0	100.9	−49.33	1168

while $V(r)$ is expressed as

$$V(r)=-d_0\left[\sum_{i=0}^{5}c_i(r-r_e)^i\right]\exp[-c_1(r-r_e)] \tag{2.4}$$

with $d_0=68.25$, $r_e=2.568$, $c_0=1$, $c_1=2.648$, $c_2=1.616$, $c_3=0.07828$, $c_4=-0.6678$, $c_5=0.3306$. The function $a_2(r)$ was fitted by

$$a_2(r)=125.10\exp[-4.205(r/5)^{3.1}]. \tag{2.5}$$

Having fitted $V(r)$, $\gamma_0(r)$, and $a_2(r)$ in such a way that the *ab initio* results for the short range MEP were reproduced, the functions $a_3(r)$ and $a_4(r)$ were chosen to reproduce the properties of the long range MEP. Here, the fit was achieved by the functions

$$a_j(r)=\left[\sum_{i=1}^{6}d_{ji}(x-x_{j0})^i\right]\frac{\exp[-\beta_j(x-x_{j0})]}{1+\exp[-1.75\beta_j(x-x_{j0})]} \tag{2.6}$$

with $j=3$ and 4, $x=\ln r$, $x_{30}=1.658$, $x_{40}=1.656$, $\beta_3=10.58$, $\beta_4=10.90$, $d_{31}=-51.05$, $d_{32}=-497.1$, $d_{33}=1912$, $d_{34}=-16735$, $d_{35}=30250$, $d_{36}=-23740$, $d_{41}=-0.4957$, $d_{42}=650.9$, $d_{43}=-4527$, $d_{44}=25460$, $d_{45}=-43450$, $d_{46}=31480$. The given analytical representation of the potential energy surface surprisingly well reproduces the *ab initio* data. For instance, the saddle point on the way between the short- and long-range MEP, from the analytical expression, has the properties $r=5.395a_0$, $\gamma=46.34°$, $V(r,\gamma)=-1.469$ kcal mol^{-1}, $\omega_1=205$ cm^{-1}, and $\omega_2=i207$ cm^{-1}, while the *ab initio* results are $r=5.38a_0$, $\gamma=46.4°$, $V(r,\gamma)=-1.46$ kcal mol^{-1} (unscaled), $\omega_1=189$ cm^{-1}, and $\omega_2=i187$ cm^{-1}.

TABLE V. CAS+1+2+QC/aug-cc-pvtz, minimum energy path for the reaction HO+O→HO$_2$($^2A'$) in Jacobi coordinates.

r/a_0	γ	$V(r)$/kcal mol^{-1}	ω(bend)/cm^{-1}
15.0	0.0	−0.03	22
12.0	0.0	−0.10	39
10.0	0.0	−0.23	68
9.0	0.0	−0.39	93
8.0	0.0	−0.70	129
7.0	0.0	−1.32	190
6.5	0.0	−1.74	221
6.0	0.0	−2.06	243
5.8	0.0	−2.07	245
5.6	0.0	−1.80	206
5.5	0.0	−1.65	197
5.4	0.0	−1.44	169
5.2	0.0	−0.72	58*i*
5.0	0.0	+0.39	236*i*
5.5	99.2	−0.71	144
5.2	96.4	−1.14	202
5.0	94.7	−1.57	251
4.8	93.6	−2.19	311
4.6	93.0	−3.06	382
4.4	92.8	−4.32	465
4.2	92.9	−6.14	559
4.0	93.3	−8.75	663
3.8	94.1	−12.39	772
3.6	95.1	−17.24	879
3.4	96.4	−23.41	982
3.0	100.0	−37.23	1132

We can also compare our results with the DMBE IV expression from Ref. 42. Figures 4 and 5 show equipotential lines of the ground state potential from the present representation of the *ab initio* results (see also Fig. 1), and from the DMBE IV representation. The two representations look qualitatively similar. However, there are quantitative differences in $V(r)$ along the MEP, similar to those observed on the H–OO side.[42] These differences are particularly harmful, as they are in a range which is most relevant for the kinetics (the DMBE IV MEP shows an almost two times stronger attraction energy at intermediate distances than our *ab initio*

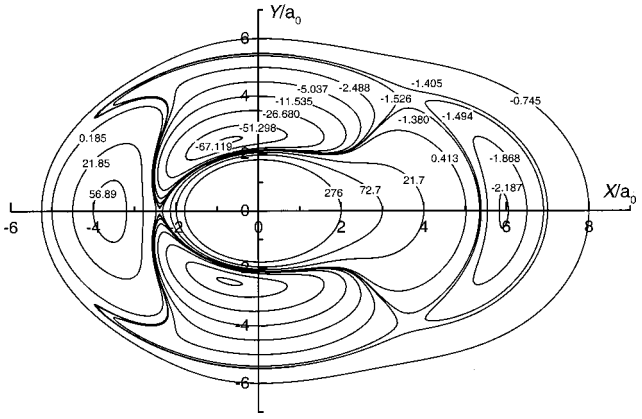

FIG. 4. Equipotential contours for the lowest electronic state ($^2A''$) of the HO+O system. Representation of the present *ab initio* results by Eqs. (2.1)–(2.6) (HO is located along the *X*-axis with the center of mass at the origin, O is located in the *X*,*Y*-plane, energies are in kcal mol^{-1}, positive values denote energies above that of reactants, negative values denote attraction).

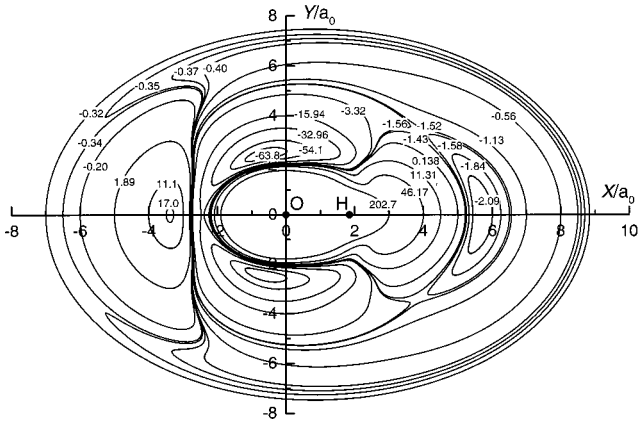

FIG. 5. As Fig. 4, representation of the DMBE IV potential from Ref. 42 (HO is located along the *X*-axis with the O atom at the origin).

results).[44] Therefore, although providing an appealing global representation of the complete potential, at intermediate interfragment distances the DMBE IV surface does not reproduce the *ab initio* results sufficiently well. The present representation, although not being globally complete, provides all details required for SACM/CT-statistical rate calculations on the accuracy level provided by the *ab initio* treatment. In addition, it has the advantage to be of much simpler form than the cumbersome DMBE IV expression.

III. CLASSICAL TRAJECTORY CALCULATIONS OF THERMAL CAPTURE RATE CONSTANTS FOR THE REACTION HO+O→HO$_2$

At first, we have calculated thermal capture rate constants k_6 by applying the method described in Ref. 73. At each temperature, about 10^4 trajectories for the approach of HO and O were studied and inspected with respect to the occurrence of capture. The number of trajectories was large enough that statistical uncertainties were negligible. Calculations were made either in the absence of an anisotropy of the MEP potential, which defines phase space theory (PST), or in the presence of the anisotropy of the real potential. The results, first, are represented in the form of a capture rate constant $k_{\rm cap}$ neglecting the statistical weights of the fine structure components of O($^3P_2$) and OH($^2\Pi_{3/2}$). The rate constant $k_{\rm cap}$ then is given by Eq. (1.7) omitting the product of the electronic partition functions. In providing the representation of $k_{\rm cap}$, one best can distinguish the different contributions of $k_{\rm cap}$ and of the electronic partition functions to the temperature dependence of k_6. Figure 6 shows the results. The temperature dependencies of $k_{\rm cap}^{\rm PST}$ and $k_{\rm cap}$ are noticeably different. Figure 7 illustrates this observation by providing the thermal rigidity factor $f_{\rm rigid}(T)=k_{\rm cap}/k_{\rm cap}^{\rm PST}$ which is a marked function of the temperature. According to our earlier work,[44,73,90] most of this temperature dependence is due to the fact that the real *ab initio* potential is not of ''uniform anisotropy character,'' such as investigated in detail in Ref. 73, but governed by the transition from an OHO to an HO$_2$ structure.

It appears useful to compare the thermal rigidity factor of Fig. 7 with the prediction for a potential of uniform stan-

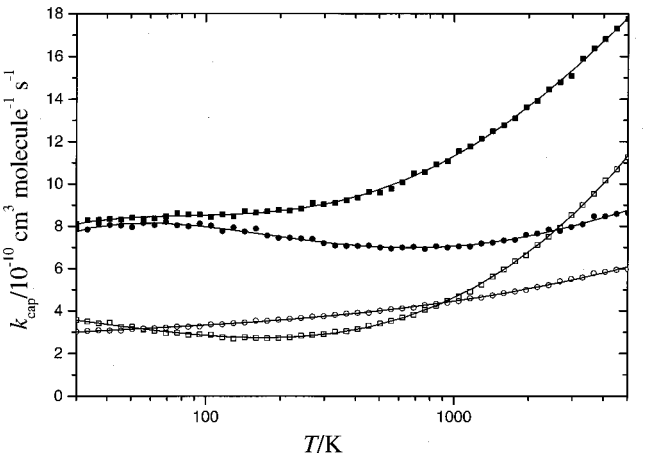

FIG. 6. Thermal capture rate constants k_{cap} for the reactions H+O$_2$→HO$_2$ (squares) and HO+O→HO$_2$ (circles) in phase space theory (filled symbols) and for the anisotropic potential (open symbols) [CT results on *ab initio* potentials, see Eqs. (3.2), (3.3), (3.6), and (3.7); electronic weight factors f_{el} omitted, see text].

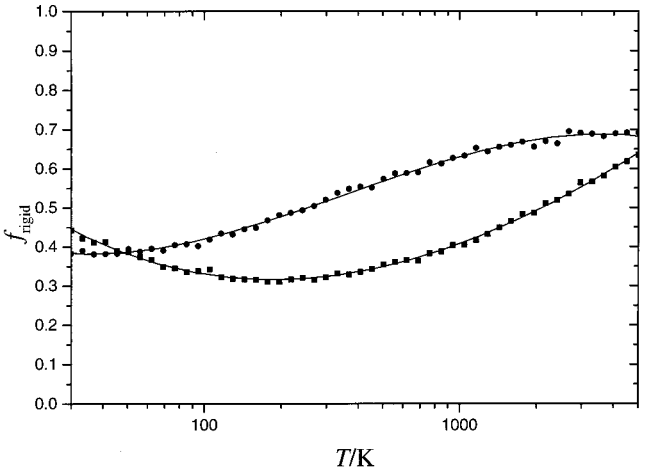

FIG. 7. Thermal rigidity factors $f_{rigid}(T)=k_{cap}/k_{cap}^{PST}$ for the reactions H+O$_2$→HO$_2$ (squares) and HO+O→HO$_2$ (circles).

dard anisotropy, see Ref. 73. In order to do this, we consider the standard anisotropy parameter C defined by

$$C=\hbar\omega(r_e)^2/2BD \tag{3.1}$$

which, with a bending quantum $\hbar\omega(r_e)\approx 1100\,\mathrm{cm}^{-1}$, $B(\mathrm{OH})=18.895\,\mathrm{cm}^{-1}$, and $D=23\,930\,\mathrm{cm}^{-1}$, leads $C\approx 1.3$. According to Eqs. (6.2) and (6.4) from Ref. 73, this would give $f_{rigid}(T\to 0)\approx 0.87$ for a linear adduct and even larger values for a transition to a T-shaped adduct. Obviously, the failure of this standard procedure reflects the complicated structure of the present potential which, in its long-range part, is more anisotropic than a simple valence potential without an outer potential minimum. Putting instead bending frequency and dissociation energy of the linear OHO shallow minimum into Eq. (3.1) [i.e., $\hbar\omega(r_e)\approx 250\,\mathrm{cm}^{-1}$, $D\approx 700\,\mathrm{cm}^{-1}$, see Figs. 2 and 3], one would have $C\approx 2.4$ which corresponds to $f_{rigid}(T\to 0)\approx 0.42$. This value is in close agreement with that from Fig. 7, indicating that the long-range anisotropy in this case governs the rigidity factor. Interestingly, the calculated rigidity factors on the O–OH side are similar to those of the O$_2$–H side of the potential, such as also included in Fig. 7.

The temperature dependence of the capture rate constants from Fig. 6 is expressed by

$$k_{cap}(\mathrm{HO+O})/10^{-10}\ \mathrm{cm}^3\,\mathrm{molecule}^{-1}\,\mathrm{s}^{-1} = 1.70+1.57\log T-0.703(\log T)^2+0.162(\log T)^3 \tag{3.2}$$

and

$$k_{cap}^{PST}(\mathrm{HO+O})/10^{-10}\ \mathrm{cm}^3\,\mathrm{molecule}^{1}\,\mathrm{s}^{-1} = -27.93+58.37\log T-33.36(\log T)^2+7.887(\log T)^3-0.6496(\log T)^4 \tag{3.3}$$

(with T in K and log=log$_{10}$). If one assumes that only capture into the $X\,^2A''$ electronic ground state of HO$_2$ contributes to k_6, one finally has

$$k_6=k_{cap}f_{el} \tag{3.4}$$

with

$$f_{el}=\frac{Q_{el}(\mathrm{HO_2})}{Q_{el}(\mathrm{O})Q_{el}(\mathrm{HO})}\approx\frac{2}{[5+3\exp(-228\ \mathrm{K}/T)+\exp(-327\ \mathrm{K}/T)][2+2\exp(-187\ \mathrm{K}/T)]}. \tag{3.5}$$

As noted before,[50] most of the temperature dependence of k_6 originates from f_{el} i.e., from the thermal population of those electronic fine structure components of O and HO which contribute to capture. It appears remarkable that the capture rate constants for reaction (1.4) from,[44]

$$k_{cap}(\mathrm{H+O_2})/10^{-10}\ \mathrm{cm}^3\ \mathrm{molecule}^{-1}\,\mathrm{s}^{-1} = 1.71+6.57\log T-5.30(\log T)^2+1.13(\log T)^3 \tag{3.6}$$

and

$$k_{cap}^{PST}(\mathrm{H+O_2})/10^{-10}\ \mathrm{cm}^3\ \mathrm{molecule}^{-1}\,\mathrm{s}^{-1} = 4.14+7.74\log T-4.82(\log T)^2+1.01(\log T)^3, \tag{3.7}$$

such as included in Figs. 6 and 7, are close to the results for reaction (1.6). However, this similarity is accidental. The much larger differences of the complete rate constants $k=k_{cap}f_{el}$ are due to the differences in f_{el} which are given by Eq. (3.5) for reaction (1.6) and by $f_{el}=1/3$ for reaction (1.4), see Ref. 44.

The present capture rate constants for the reaction HO+O are fairly close to the simplified SACM calculations from Ref. 50. In this previous work, a long-range/short-range switching potential was constructed, which at long ranges included dipole–quadrupole, quadrupole–quadrupole, and dispersion contributions, and which at short ranges used a simplified Morse-type *ab initio* potential from Ref. 52. Although this simple potential model did not explicitly account for the complicated outer OHO potential minimum, the essential features of the attraction between O and HO and of the corresponding anisotropy of the potential were well reproduced. $k_{cap}^{PST} \approx 6 \times 10^{-10}\,cm^3\,molecule^{-1}\,s^{-1}$ and $k_{cap} \approx 2 \times 10^{-10}\,cm^3\,molecule^{-1}\,s^{-1}$ were obtained nearly independent of the temperature. The close agreement with the present much more detailed treatment appears worth noticing. On the other hand, a treatment following,[73] using a simple standard valence potential without long-range contributions, see Eq. (3.1), would lead to larger differences which illustrates the unusual potential of the O+HO reaction system.

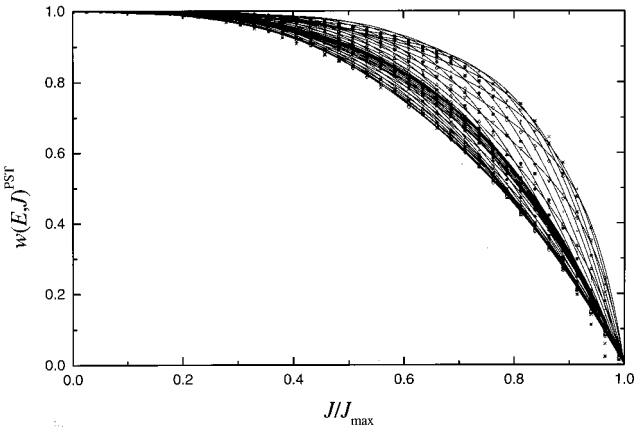

FIG. 8. *E*- and *J*-specific capture probabilities $w(E,J)^{PST}$ in phase space theory for the reaction $HO+O \rightarrow HO_2$. [$J_{max}(E)$ given by Eqs. (4.7)–(4.9), energies *E* of the curves = 10–30 000 cm^{-1} from the middle to the top, then to the bottom, and finally to the middle again; symbols of energies as in Figs. 8 and 10 of Ref. 44 for the reaction $H+O_2 \rightarrow HO_2$.]

IV. CLASSICAL TRAJECTORY CALCULATIONS OF *E*- AND *J*-SPECIFIC CAPTURE PROBABILITIES, SPECIFIC DISSOCIATION RATE CONSTANTS OF HO_2, AND THERMAL RATE CONSTANTS FOR THE REACTION $H+O_2 \Leftrightarrow HO+O$

In the following we explicitly investigate the question to what extent the complex-forming bimolecular reaction (1.1) is capture-controlled such that $k_1 \approx k_6$. Reaction (1.1) is a classical example of a loose entrance/loose exit reaction system[91] for which capture

$$HO+O \rightarrow HO_2^* \tag{4.1}$$

is followed by a competition between the two unimolecular dissociations of the intermediate HO_2 complex,

$$HO_2^* \rightarrow HO+O, \tag{4.2}$$

$$HO_2^* \rightarrow H+O_2. \tag{4.3}$$

The simplified SACM treatment from Ref. 50 indicated that back-dissociation (4.2) only at high temperatures (above about 1000 K) noticeably reduces k_1 below k_6. On the other hand, the QCT calculations from Ref. 54 suggested marked back-dissociation for all temperatures. In the present section, we determine *E*- and *J*-specific rate constants for reaction (4.2), to be compared with the corresponding quantities for reaction (4.3) such as treated in Ref. 44. Going beyond the potential model from Ref. 50, with the present *ab initio* potential we elaborate the finer details of the numbers of open channels $W_a(E,J)$ for reaction (4.2), in comparison to $W_b(E,J)$ for reaction (4.3) from Ref. 44.

Our procedure follows the method outlined in Ref. 44. We first calculate the number $W_0(E,J)$ of quantum states of a free rotor and an atom, at a given energy *E* and total angular momentum (quantum number *J*). At this stage we neglect electronic spins and electronic angular momenta. $W_0(E,J)$ is given by[92]

$$W_0(E,J) = (2J+1)(j_{max}+1) - J(J+1) \tag{4.4}$$

for $0 \leqslant J \leqslant j_{max}$ and

$$W_0(E,J) = (j_{max}+1)^2 \tag{4.5}$$

for $J \geqslant j_{max}$, where j_{max} is the largest *j* with $0 \leqslant Bj(j+1) \leqslant E$ (B = rotational constant of the free rotor). By classical trajectory calculations we then determine classical capture probabilities $w(E,J)$, being the fractions of trajectories which, from a given *E* and *J*, lead to capture. We used the following capture criterion: The sum of the MEP potential $V(r)$ from Sec. II and the centrifugal energy has an inner minimum at the energy *E*; this minimum is located at a value of $r = r_c$. All trajectories reaching $r \leqslant r_c$ then are counted as leading to capture. The results for $w(E,J)$ only very mildly depend on small modifications of the capture criterion. Numbers of open channels for complex formation (or complex dissociation) $W(E,J)$ finally are given by

$$W(E,J) = w(E,J)W_0(E,J). \tag{4.6}$$

''Empirical quantization'' is achieved by rounding up or down the noninteger $W(E,J)$. This procedure in comparison to true quantum SACM leaves only very minor differences,[75] see also below.

Because of the complicated structure of the potential on the O–OH side, our calculated quantities are difficult to represent in analytical form. Only a graphical representation of the results is given here. At first, Fig. 8 shows capture probabilities $w(E,J)^{PST}$ in phase space theory. The horizontal axis is scaled by the maximum possible *J*-value allowing for the overcoming of the centrifugal barrier (which is termed J_{max}). An analytical representation of J_{max} is provided by

$$\ln J_{max} = c_1 + c_2 x + c_3 x^2 \tag{4.7}$$

at $\ln E < x_0$, with $x = \ln E - x_0$, E in cm^{-1}, $x_0 = 4.602$; $c_1 = 3.917$, $c_2 = 0.275$, $c_3 = -0.00345$,

$$\ln J_{max} = c_1 - c_6 + c_4 x + c_5 x^2 + [c_6 + c_7 x + c_8 x^2] \times \exp(-c_9 x) \tag{4.8}$$

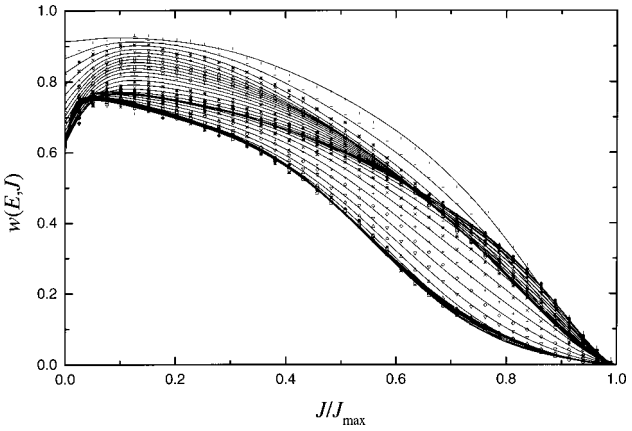

FIG. 9. E- and J-specific capture probabilities $w(E,J)$ with the anisotropic potential for the reaction HO+O→HO$_2$ (energies E of the curves $=10-30\,000\ \mathrm{cm}^{-1}$ from bottom to top, symbols as in Fig. 8).

at $x_0 \leqslant \ln E \leqslant x_1$, with $x=\ln E-x_0$, $x_1=9.815$, $c_4=0.191$, $c_5=0.00813$, $c_6=-0.406$, $c_7=-0.373$, $c_8=-0.307$, $c_9=0.818$,

$$\ln J_{\max}=c_{10}+c_{11}x+c_{12}x^2, \tag{4.9}$$

at $\ln E>x_1$, with $x=\ln E-x_1$, $c_{10}=5.392$, $c_{11}=0.204$, $c_{12}=-0.100$. The curves for $w(E,J)^{\mathrm{PST}}$ at low energies are in the middle of the dense group of curves; with increasing energy they move to the top, then to the bottom, and finally end up again in the middle of the dense group of curves. Figure 9 provides the capture probabilities $w(E,J)$ for the complete anisotropic potential, with energies being between 10 at the bottom and 30 000 cm^{-1} at the top of the dense group of curves. In order to illustrate the effects of the anisotropy of the potential, in Fig. 10 we also show the E- and J-specific rigidity factors $f_{\mathrm{rigid}}=w(E,J)/w(E,J)^{\mathrm{PST}}$. In spite of the complicated structure, the comparison with the corresponding curves for the H–O$_2$ side (see Ref. 44), shows a surprisingly similar general behavior.

Combining numbers of states $W_0(E,J)$, for the free rotor and the atom, with the capture probabilities $w(E,J)$ through Eq. (4.6) leads to the numbers of open channels

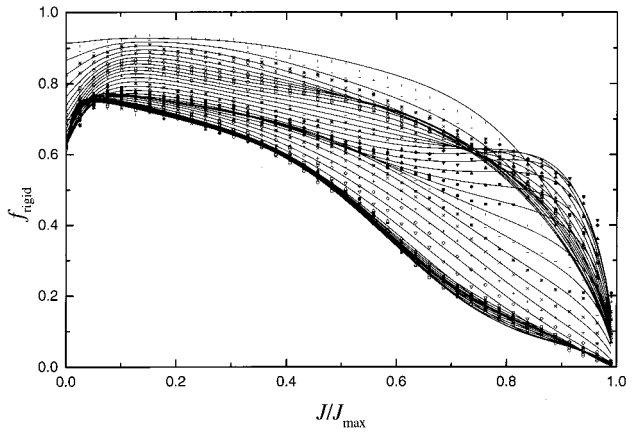

FIG. 10. E- and J-specific rigidity factors $f_{\mathrm{rigid}}(E,J)$ for the reaction HO+O→HO$_2$ (energies E of the curves$=10-30\,000\ \mathrm{cm}^{-1}$ from bottom to top, symbols as in Fig. 8).

TABLE VI. Specific rate constants $k(E,J)$, anharmonic vibrational densities of states $\rho(E,J)$, and total numbers of open channels $W(E,J)$ for the dissociation HO$_2$→H+O$_2$ [$E=0$ at dissociation threshold, statistical theory with $k(E,J)=W(E,J)/h\rho(E,J)$].

E/cm^{-1}	$k(E,J)/10^{12}\,\mathrm{s}^{-1}$	$\rho(E,J)/\mathrm{cm}$	$W(E,J)$
	$J=0$		
10.00	0.462	0.065	1
19.95	0.461	0.065	1
39.79	0.457	0.066	1
79.37	0.450	0.067	1
158.32	0.437	0.069	1
315.81	0.821	0.073	2
629.96	0.723	0.083	2
1256.61	1.122	0.107	4
2506.60	1.772	0.169	10
5000.00	2.367	0.342	27
	$J=10$		
37.45	0.024	1.232	1
64.51	0.048	1.245	2
111.12	0.118	1.267	5
191.40	0.230	1.306	10
329.70	0.370	1.378	17
567.92	0.613	1.517	31
978.27	0.868	1.795	52
1685.12	1.132	2.384	90
2902.69	1.706	3.674	209
5000.00	2.245	6.624	496
	$J=20$		
228.58	0.016	1.846	1
322.05	0.016	1.912	1
453.73	0.089	2.010	6
639.27	0.222	2.163	16
900.67	0.411	2.409	33
1268.95	0.629	2.812	59
1787.83	0.825	3.489	96
2518.88	1.235	4.636	191
3548.86	1.609	6.597	354
5000.00	2.026	10.020	677
	$J=40$		
1324.77	0.016	1.867	1
1535.44	0.030	2.023	2
1779.61	0.135	2.222	10
2062.61	0.289	2.494	24
2390.61	0.450	2.866	43
2770.77	0.602	3.388	68
3211.39	0.772	4.076	105
3722.08	1.029	5.014	172
4313.98	1.269	6.237	264
5000.00	1.514	7.883	398

$W_a(E,J)$ for reaction (4.2). Finally, $W_a(E,J)$ such as derived for the ''transitional modes'' is convoluted with the contribution from the ''conserved mode.'' In the present case, this mode is represented sufficiently well by the vibration of the free HO radical.[92] We tabulate representative results in Table VI. For comparison, we also give $W_b(E,J)$ for reaction (4.3) in Table VII. According to Eq. (1.9), the ratio $W_b(E,J)/[W_a(E,J)+W_b(E,J)]$ enters the final expression for k_2. Figure 11 shows this ratio which, in our statistical theory, is equal to the probability of H+O$_2$-formation after HO$_2^*$ has been formed by HO+O capture. At small energies nearly all complexes lead to reaction, at large energies there

TABLE VII. As Table VI for the dissociation $HO_2 \rightarrow HO+O$.

E/cm^{-1}	$k(E,J)/10^{12}\,s^{-1}$	$\rho(E,J)$/cm	$W(E,J)$
	$J=0$		
10.00	0.072	0.416	1
19.95	0.072	0.417	1
39.79	0.072	0.418	1
79.37	0.071	0.422	1
158.32	0.140	0.429	2
315.81	0.203	0.444	3
629.96	0.253	0.474	4
1256.61	0.279	0.538	5
2506.60	0.354	0.678	8
5000.00	0.472	1.016	16
	$J=10$		
10.00	0.004	8.086	1
19.95	0.004	8.104	1
39.79	0.011	8.140	3
79.37	0.011	8.213	3
158.32	0.022	8.357	6
315.81	0.042	8.651	12
629.96	0.088	9.252	27
1256.61	0.140	10.520	49
2506.60	0.254	13.325	113
5000.00	0.370	20.098	248
	$J=30$		
15.99	0.002	12.499	1
30.27	0.002	12.545	1
57.31	0.002	12.634	1
108.51	0.002	12.802	1
205.46	0.009	13.125	4
389.03	0.033	13.748	15
736.59	0.048	14.974	24
1394.68	0.098	17.465	57
2640.72	0.146	22.812	111
5000.00	0.226	35.398	267
	$J=60$		
356.99	0.005	5.573	1
478.66	0.010	5.826	2
641.79	0.034	6.178	7
860.52	0.072	6.667	16
1153.80	0.106	7.358	26
1547.03	0.136	8.377	38
2074.27	0.162	9.821	53
2781.21	0.215	12.006	86
3729.08	0.251	15.283	128
5000.00	0.316	20.500	216

is considerable back reaction. The consequence, after thermal averaging according to Eq. (1.9), is a decrease of k_2 below k_6 which becomes increasingly more pronounced with increasing temperatures, see Fig. 12. A minor additional correction at low temperatures has been introduced by replacing the classical rotational partition function of HO in Eq. (1.9) by its quantum analog, see below.

Tables VI and VII also provide specific rate constants $k_a(E,J)$ and $k_b(E,J)$ for the two dissociation channels (4.2) and (4.3) such as calculated on the basis of the derived $W_a(E,J)$ and $W_b(E,J)$ from Eq. (1.11). Figure 13 combines the specific rate constants in one representation (putting the zero of the energy scale at the ground level of $H+O_2$). A number of points should be noted: The curves show the opening of new vibrational states of O_2 in $k_b(E,J)$, or of HO

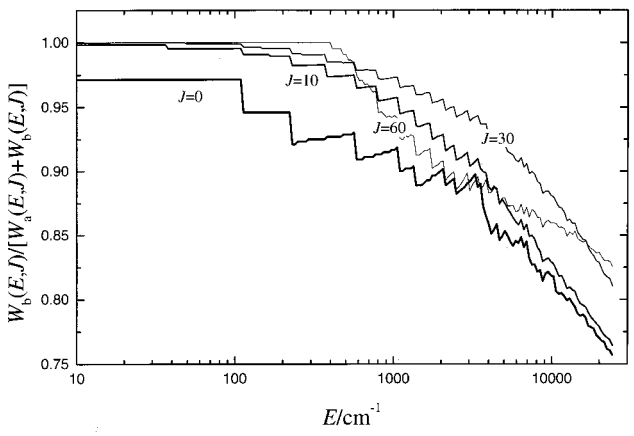

FIG. 11. E- and J-specific product yield $W_b(E,J)/[W_a(E,J)+W_b(E,J)]$ in Eq. (1.9) [subscript ''b'' for $H+O_2 \Leftrightarrow HO_2$, subscript ''$a$'' for $HO+O \Leftrightarrow HO_2$; $W(E,J)$ = number of open channels, see Tables VI and VII].

in $k_a(E,J)$. $W_b(E,J)$ as well as the rotational partition functions of O_2 are both divided by a factor $\sigma=2$ because of the nuclear spin statistics of O_2. The rovibrational densities of states $\rho(E,J)$ in Eq. (1.11) have been modified considerably compared to our earlier work. Vibrational anharmonicity factors $F_{anh}(E)$, to be multiplied with the ''harmonic'' densities of states (using the experimental fundamental frequencies of HO_2, 3436.20, 1391.75, and 1097.63 cm^{-1} from Ref. 93), have been calculated following the method from Ref. 94. This leads to an expression for $F_{anh}(E)$ of

$$F_{anh}(E) \approx 1 + a(E-\Delta H_0) + \sqrt{a^2(E-\Delta H_0)^2+0.6} \tag{4.10}$$

with $\Delta H_0 = 16\,650\,cm^{-1}$, $a = 4.83\times10^{-4}/cm^{-1}$, and the energy E above the ground state of $H+O_2$. Rovibrational densities of states were determined by explicit summation

$$\rho(E,J) = \sum_{K=-J}^{J} g(K)\rho_{vib}(E-BJ(J+1)-(A-B)K^2) \tag{4.11}$$

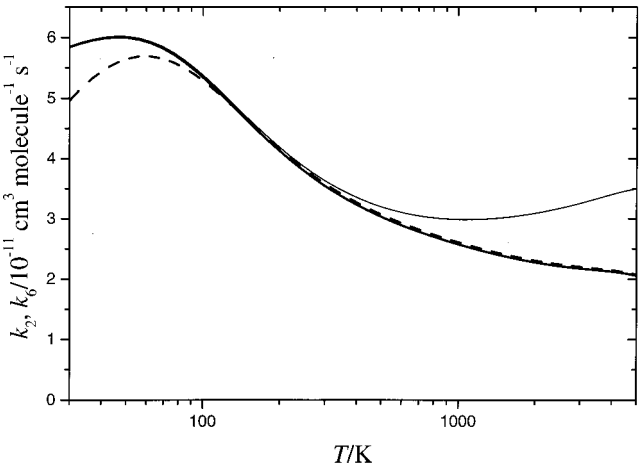

FIG. 12. Calculated thermal rate constants k_6 (for $HO+O \rightarrow HO_2$, heavy lines) and k_2 (for $HO+O \rightarrow H+O_2$, light line) (CT calculations from this work on *ab initio* potential; full line=fully classical results, dashed line=with quantum rotational partition function of HO).

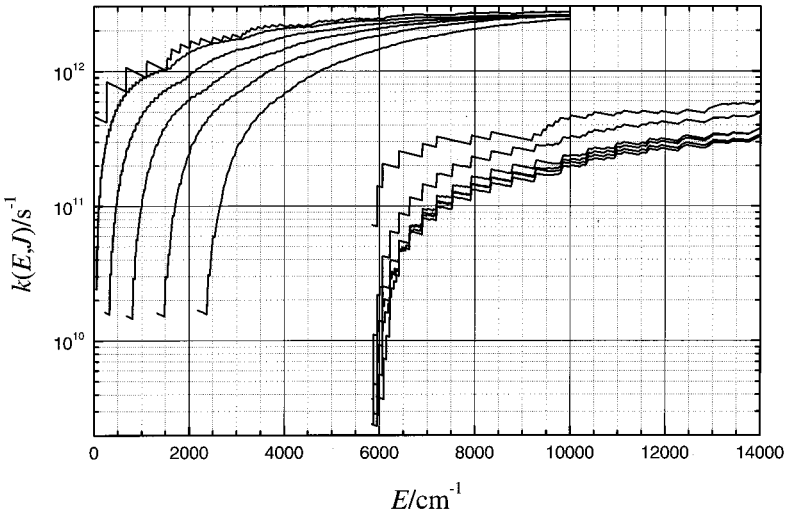

FIG. 13. Specific rate constants $k(E,J)$ for $HO_2 \rightarrow H+O_2$ (left group of curves) and for $HO_2 \rightarrow HO+O$ (right group of curves) ($E=0$ at threshold for $HO_2 \rightarrow H+O_2$; $J=0$, 10, 20, 30, 40, and 50 from top to bottom for $HO_2 \rightarrow H+O_2$; $J=0,10,50,20,40,30$ at $E=11\,000\,cm^{-1}$ for $HO_2 \rightarrow HO+O$, see Tables VI and VII).

with $g(K)=2$ for $J\neq 0$, $g(K=0)=1$, the anharmonic vibrational density of states ρ_{vib} of HO_2, and the rotational constants A and B of HO_2. Our new determination of the specific rate constants $k_a(E,J)$ and $k_b(E,J)$, because of markedly changed $\rho(E,J)$, supersedes our earlier results (Refs. 19, 44, and 50) while the earlier calculations of k_2, k_3, and k_6 from Ref. 50, employing only $W_a(E,J)$ and $W_b(E,J)$ are only mildly modified by the present more detailed calculations.

V. ADIABATIC CHANNEL POTENTIAL CURVES AND LOW TEMPERATURE CAPTURE RATE CONSTANTS FOR THE REACTION HO+O→HO$_2$

Quantum effects in low temperature capture processes can conveniently be accounted for by rigorous SACM calculations, see, e.g., Refs. 73, 75, 77, 92. The deviations of the capture rate constants k_{cap} from their classical values k_{cap}^{cl} are governed by the rotational constants B of the rotor reactant in relation to kT, and by the effective anisotropy parameters C of the potential, see Eq. (3.1). For the capture process $H+O_2 \rightarrow HO_2$, the *ab initio* calculations of the potential from Ref. 44 indicate that the effective value of C is not independent of the distance r_{H-O_2} between $H+O_2$. Taking into account[44] that $f_{rigid} \geqslant 0.45$ at $T \leqslant 30$ K and that the MEP approaches a linear HO_2 structure at large r_{H-O_2}, the effective anisotropy of the potential for $T \leqslant 30$ K corresponds to $C<3$. According to the quantum SACM calculations from Ref. 73, one then has $k_{cap} \approx k_{cap}^{cl}$ down to temperatures below $T=B/k \approx 2$ K. We, therefore, do not further elaborate quantum effects for $H+O_2$ capture at this place. More detailed *ab initio* calculations of the potential at very long range ($r_{H-O_2} > 10a_0$) anyway would be required for a more precise calculation of $k_{cap}(H+O_2)$ at $T<2$ K.

Because of the larger rotational constant of HO($B/k=27.15$ K) and because of its open shell nature, quantum effects in k_{cap} will reach up to much higher temperatures for $HO+O \rightarrow HO_2$ than for $H+O_2 \rightarrow HO_2$. The effective C of the linear shallow OHO minimum of the potential was estimated to be near $C \approx 2.4$, see above. According to the calculations from Ref. 73, for closed shell systems, a potential of this anisotropy is characterized by adiabatic zeropoint barriers of the magnitude,

$$\frac{E_0(l=0)}{B} \approx \frac{3}{2}\left[\frac{C-2}{C}+0.47\left(\frac{C-2}{C}\right)^{3.43}\right]^2, \tag{5.1}$$

which leads to $E_0(l=0)/B \approx 0.168$. As a consequence, the quantum capture rate constant, which, according to Ref. 73, approaches $k_{cap}(T\rightarrow 0) \propto T^{1/2} \exp[-E_0(l=0)/kT]$ should go to zero at $T\rightarrow 0$ K. The open shell nature of HO will modify this effect, producing quantum effects at even higher temperatures and changing $k_{cap}(T\rightarrow 0\ K)$ (Refs. 77 and 92), see below. In order to obtain quantitative data, we have calculated adiabatic channel potential curves for the present *ab initio* potential, at first neglecting the open shell nature of HO($^2\Pi_{3/2}$) and O($^3P_2$). The determination of the positions of the channel maxima shows that the potential of the OHO intermediate structure governs most channel maxima. Specifying the channels by their limiting quantum numbers j and m,[92] the l-dependence of the individual channel maxima $E_0(l)$ is represented by the expressions given in the Appendix. The corresponding limiting low temperature capture rate constant is illustrated in Fig. 14. The figure includes the capture rate constants k_{cap}^{cl} from our classical trajectory calculations, see Eq. (3.2), however, employing the correct quantum rotational partition function of HO instead of the classical rotational partition function, see also Fig. 12. From the described quantum SACM calculations, we first show results, $k_{cap}^{SACM}(j=0)$, including channels with $j(HO)=0$ only and putting $Q_{rot}(HO)=1$; in addition, results, $k_{cap}^{SACM}(J=0,1)$ including channels with $j(HO)=0$ and 1 are shown, employing the complete quantum rotational partition function. The adiabatic zero point barrier of the lowest channel with $j=0$ indeed forces $k_{cap}(T\rightarrow 0\ K)$ down to zero. Calculations with the channel for $j=0$ suffice for temperatures below 10 K. The agreement between the SACM results (including channels with $j=0,1$) and the CT results above 30 K is satisfactory although $k_{cap}^{SACM}(j=0,1)$ at higher temperatures starts falling below k_{cap}^{cl} because channels with larger j have not

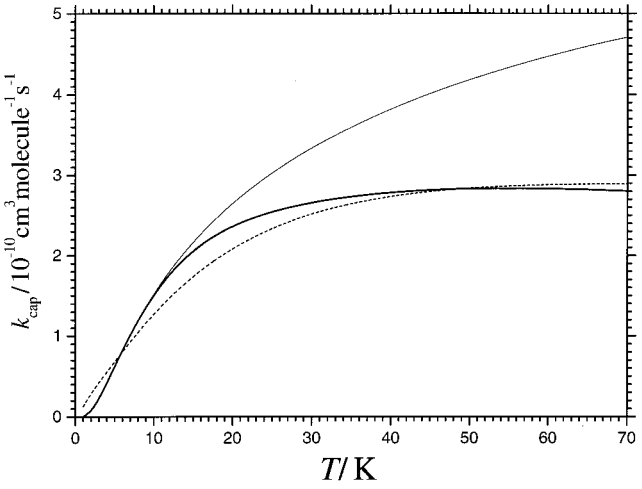

FIG. 14. Comparison of rate constants k_{cap} for closed shell capture $HO+O \rightarrow HO_2$ [see Eq. (3.4)] from classical CT calculations (dashed line, k_{cap}^{cl} employing quantum rotational partition function of HO) and quantum SACM calculations [light full line, $k_{cap}^{SACM}(j=0)$; heavy full line, $k_{cap}^{SACM}(j=0,1)$, see text].

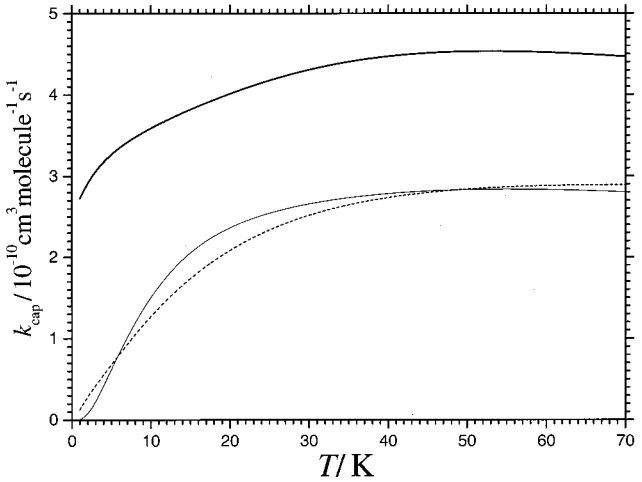

FIG. 15. Comparison of rate constants k_{cap} for closed shell capture $HO+O \rightarrow HO_2$ [dashed line, k_{cap}^{cl} from CT calculations; light full line, $k_{cap}^{SACM}(j=0,1)$] and for open shell capture $HO(^2\Pi_{3/2})+O \rightarrow HO_2$ [heavy full line, k_{cap}^{SACM} ($j=3/2$, $|m|=1/2,3/2$), see text].

been included. [It should be remembered that electronic population factors f_{el} from Eq. (3.5) are not included in k_{cap}.]

The picture changes markedly when the open shell nature of the system is taken into account. At present, we have only considered the open shell nature of $HO(^2\Pi_{3/2})$ and neglected that of $O(^3P_2)$, except the fivefold degeneracy. Therefore, our results are not rigorous; they have to treat all degenerate electronic states with the corresponding mixing of angular momentum projections, see Ref. 49. However, we do not expect major changes when the electronic degeneracy is treated correctly. The largest electronic effects probably are accounted for in the electronic population factor f_{el} from Eq. (3.5) which will be multiplied with k_{cap} later on. The channels are now specified by noninteger limiting quantum numbers j and m. The l-dependence of the individual channel maxima $E_0(l)$ again is represented in the Appendix. Different from the closed shell treatment, one channel (the channel with $j=m=+3/2$) has no adiabatic zeropoint barrier. As a consequence, in contrast to the closed shell treatment, $k_{cap}(T \rightarrow 0\ \mathrm{K})$ does not go to zero. With increasing temperature, also the channels with $j=3/2$, $m=-3/2$, and $|m|=1/2$ contribute. Figure 15 shows k_{cap}^{SACM} ($j=3/2$, $|m|=1/2,3/2$), including the eight lowest channels of $HO(^2\Pi_{3/2})$ with $j=3/2$, but employing the complete quantum rotational partition function of $HO(^2\Pi_{3/2})$. One observes that k_{cap}^{SACM} ($j=3/2$, $|m|=1/2,3/2$) at 70 K exceeds the closed shell result by about 50%. Because the accurate open shell adiabatic channel calculations with the relevant part of the complicated OHO potential are fairly cumbersome and so far we have treated structureless O atoms only, we have not done calculations for higher channels. Therefore, our results for k_{cap}^{SACM} at present cannot be extended to temperatures much above 70 K. However, it will be shown in Sec. VI B that the extrapolation of the open shell results, after conversion into k_6 with Eqs. (3.4) and (3.5), meets very well with experimental data reaching down to 160 K which validates the present treatment.

The described low temperature calculations of k_6 differ considerably from the results of ''rotationally adiabatic perturbation theory'' such as elaborated in Refs. 95–97 which led to a rate constant of $2.56\times10^{-10}\,\mathrm{cm^3\,molecule^{-1}\,s^{-1}}$ at $T\rightarrow0$ K, in contrast to the present value of $2.6\times10^{-11}\,\mathrm{cm^3\,molecule^{-1}\,s^{-1}}$. There are several reasons for this discrepancy: without *ab initio* calculations one cannot decide which potentials out of the electronic mainfold lead to reaction (in the present case this is one-fifth); in addition a long-range dipole–quadrupole potential in the present case is not sufficient for calculating k_6, because the true OHO/HOO potential influences the temperature dependence down to very low temperatures. The perturbation treatment, therefore, quite generally does not appear appropriate for predictions of rate constants for reactions between open shell neutral species under astrophysical conditions. One should note that the reaction O+HO is being discussed as a possible process in interstellar chemistry being of interest under dense cloud conditions in the 10–20 K temperature range.[98]

VI. DISCUSSION

A. Specific rate constants $k(E,J)$ for the dissociations of HO_2

Specific rate constants $k(E,J=0)$ for HO_2 dissociation into $H+O_2$ have been calculated in Ref. 69 using wave packet dynamics, classical trajectories and simple RRKM calculations on the DMBE IV surface. Although being restricted to $J=0$, these results can be compared with our present calculations of $k(E,J)$. The wave packet calculations from Ref. 69 show considerable fluctuations of $k(E,J=0)$, near threshold between 2×10^8 and $3\times10^{12}\,\mathrm{s^{-1}}$, and at an energy 4000 $\mathrm{cm^{-1}}$ above threshold between 10^{12} and $5\times10^{12}\,\mathrm{s^{-1}}$. The average of these rate constants increases from about 5.5×10^{11} at threshold to about $4\times10^{12}\,\mathrm{s^{-1}}$ at 4000 $\mathrm{cm^{-1}}$ above threshold, in close agreement with trajec-

tory and RRKM results. Our present data range from 4.7 $\times 10^{11}$ near threshold to $2.2\times 10^{12}\,s^{-1}$ at 4000 cm^{-1} above threshold, see Table VI. The reason for the minor differences of $k(E,J=0)$ between[69] and the present results is easily traced. In the present work, $\rho(E_0)=0.064/cm^{-1}$ and $\rho(E_0+4000\,cm^{-1})=0.31/cm^{-1}$ is determined using the anharmonicity calculation from Ref. 79. Instead, $\rho(E_0)=0.055/cm^{-1}$ and $\rho(E_0+4000\,cm^{-1})=0.085/cm^{-1}$ was derived in Ref. 69 by phase space integration up to E_0 and simple extrapolation towards higher energies. The latter procedure does not appear to be adequate in the present case. Most of the differences in $k(E_0+4000\,cm^{-1},J=0)$ are, therefore, due to differences in the densities of states above threshold while there is close agreement at threshold. After accounting for the different densities of states, the present results still show a somewhat slower increase of $k(E,J=0)$ with increasing energy than observed in the wave packet calculations from Ref. 69. This difference can be attributed to the differences between the potential energy surfaces used in the two calculations. Indications of a ''non-RRKM behavior'' on the H+O$_2$-side of the potential are not found in Ref. 69.

The comparison of the $k(E,J)$-curves of the two dissociations of HO_2, into H+O$_2$ and HO+O, in Fig. 13 appears instructive. There is only little crossing of various $k(E,J)$-curves for H+O$_2$-formation, whereas curves for HO+O-formation are congested and are crossing at $J=20-50$. The H+O$_2$-curves are also much wider spread along the energy scale than the HO+O-curves. This difference is caused by the different J-dependencies of the centrifugal barriers $E_0(J)$, much larger barriers being found for the H+O$_2$-channel than for the HO+O-channel as a consequence of the different reduced moments of inertia of the two fragment pairs. We are not aware of other $k(E,J)$-calculations to be compared with our present results (apart from our own from Refs. 29 and 50 which are superseded by the present work).

B. Low temperature rate contants for the reaction HO+O→H+O$_2$

The low temperature measurements of k_2 between 160 and 500 K from Refs. 3–6, which according to the present analysis are dominated by the capture-controlled reaction (1.6), are satisfactorily consistent with the present open shell SACM calculations. Figure 16 compares experiments and theory. On the experimental side, we favor the values from Refs. 3 and 6 over the probably less accurate earlier values, because the latter in part may have been influenced by the presence of some secondary processes of HO (Ref. 99) [work before 1983 (Ref. 100) led to rate constants $k_2(300\,K)$ = in the range $(3-5)\times 10^{-11}\,cm^3\,molecule^{-1}\,s^{-1}$, in general agreement with our results]. On the theoretical side, we combine Figs. 12 and 15 with Eqs. (3.4) and (3.5).

In view of the present agreement between experiment and theory, a number of conclusions may be drawn.

(i) There is no evidence that the electronically excited $^2A'$-state of HO_2 contributes to reaction (1.3);

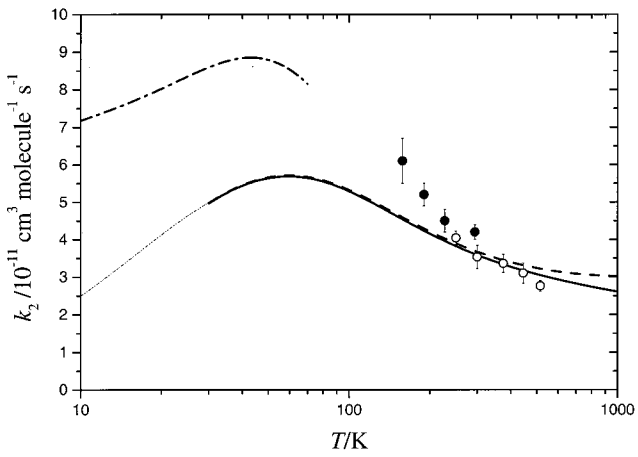

FIG. 16. Comparison of experimental and theoretical values of k_2: ●, experiments from Ref. 6; ○, experiments from Ref. 3; dashed line, CT calculations for HO+O→HO$_2$ (k_6, employing quantum rotational partition function of HO); full line, CT calculations for HO+O→H+O$_2$(k_2); light dashed–dotted–dotted line, closed shell SACM/CT calculations for HO+O→H+O$_2$(k_2); heavy dashed–dotted line, open shell SACM calculations for HO($^2\Pi_{3/2}$)+O→HO$_2$.

(ii) The present *ab initio* calculations of the potential on the HO+O-side appear to be sufficiently accurate;

(iii) There is no evidence for nonstatistical (''non-RRKM'') behavior of the reaction such as suggested in Refs. 42 and 54;

(iv) The negative temperature coefficient of k_2 between 300 and 500 K is essentially due to the temperature dependence of the thermal population f_{el} of electronic states of HO and O given by Eq. (3.5). Only at higher temperatures, back dissociation of the HO_2 adduct becomes relevant.

Previous theoretical modelings were less successful or were blessed by cancellation of errors. The most interesting point of controversy is the question whether there is nonstatistical (or ''non-RRKM'') behavior or not. The classical trajectory calculations from Refs. 48 and 54 indicate that roughly 50% of the trajectories starting from HO+O return in spite of the large exothermicity of reaction (1.1), the fraction of recrossing trajectories being only weakly temperature dependent between 200 and 5000 K (apart from the statistical back-dissociation indicated in Fig. 12). On the other hand, the trajectory calculations of Refs. 42 and 54, employing the DMBE IV surface, lead to reasonable agreement with the experiments. We believe that this agreement is accidental and due to the cancellation of two errors (about a factor of 0.5 from recrossing and a factor of 2 from the too strong attraction of the DMBE IV surface).

One will ask what could have gone wrong in the trajectory calculations from Refs. 42 and 54. We believe that there is an unfortunate consequence of the zero point energy problem in the QCT calculations which is specific for the HO+O system. If HO is allowed to vibrate classically, trajectories may be caught in the shallow linear OHO potential minimum and in part be led to redissociation. In other words, the system behaves as a multiple-well complex-forming bimolecu-

lar reaction following the sequence $O+HO \Leftrightarrow OHO \Leftrightarrow HO_2 \rightarrow H+O_2$. The present SACM/CT treatment avoids the problem by calculating trajectories with rigid rotor HO. In this case there is no possibility of bend–stretch mixing in the OHO intermediate that could lead to recrossing. Suspicions of this kind have also been raised in Ref. 54; the inadequacy of the DMBE IV potential surface also has been noted in Refs. 48 and 54. Although we cannot prove that this analysis of the problem is correct, the quality of the present *ab initio* potential on the $H+O_2$- and on the HO+O-side and the adequateness of the method of the rate calculation apparently have resulted in satisfactory agreement between experiment and theory, both for k_2 and k_4.

For very low temperatures, additional open shell SACM calculations will be required beyond the results from Sec. V. On the one hand, the consequence of replacing the structureless O atom by $O(^3P_2)$ will have to be explored. On the other hand, higher channels with $j>3/2$ will have to be included in order to approach the classical values of the rate constants at temperatures near to 300 K. These calculations may follow the methods elaborated in Refs. 49, 77, 101, 102.

C. High temperature rate constants for the reaction $H+O_2 \rightarrow HO+O$

The numerous investigations of reaction (1.1) have provided an extensive data base for establishing k_1. A variety of different techniques have been applied and the general consensus about k_1 is more or less satisfactory. Selecting four sets of data between 960 and 5300 K,[12,13,16,17] a combined expression

$$k_1=(1.62\pm0.12) \times 10^{-10} \exp[-(7474\pm122)\mathrm{K}/T]\ \mathrm{cm^3\,molecule^{-1}\,s^{-1}} \tag{6.1}$$

was constructed in Ref. 17; no deviation from an Arrhenius form was noticed. However, there are some results which are lower than Eq. (6.1) by more than the error limits of Eq. (6.1); e.g., the data from Ref. 15 between 1050 and 2700 K are expressed as

$$k_1=(4.37\pm0.53)\times10^{-10}(T/1000\,\mathrm{K})^{-0.927} \times \exp[-8493\,\mathrm{K}/T]\ \mathrm{cm^3\,molecule^{-1}\,s^{-1}}. \tag{6.2}$$

In addition, a group of measurements provided higher values of k_1, e.g., the data from Ref. 9, obtained between 1700 and 2500 K, correspond to

$$k_1=(4.05\pm0.55) \times 10^{-10} \exp[-(8696\pm265)\,\mathrm{K}/T]\ \mathrm{cm^3\,molecule^{-1}\,s^{-1}}. \tag{6.3}$$

Although the differences between the various groups of measurements are not too large, being $\pm 50\%$ near 3000 K, in view of the large sensitivity of combustion systems with respect to k_1, every possible effort has to be directed towards improvements of its reliability. New direct measurements of k_1 with simultaneous monitoring of H, O, and HO are underway,[103] hopefully settling the problem from the experimental side. On the other hand, the good agreement between experimental and the present theoretical determinations of k_2 suggests that theory also may help to clarify the situation.

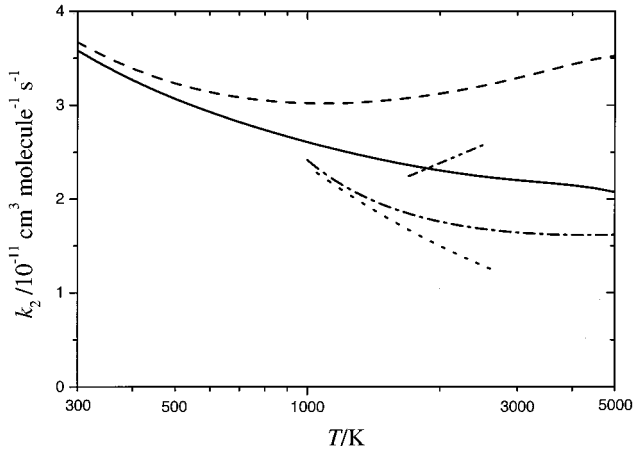

FIG. 17. Comparison of experimental and theoretical values of k_1, after conversion into k_2 with K_{eq} from Eq. (6.4) [dashed line, CT calculations of k_6; full line, CT calculations of k_2; dashed–dotted line, Eq. (6.1) (Refs. 12, 13, 16, 17); dotted line, Eq. (6.2) (Ref. 15); dashed–dotted–dotted line, Eq. (6.3) (Ref. 9)].

In order to proceed in this direction, the experimental results for k_1 have to be converted to k_2 through Eq. (1.3) using the equilibrium constant K_{eq}, while the theoretical calculations have to select the enthalpy of reaction (1.1). The precision of either quantity is dominated by the uncertainty of the enthalpy of formation of HO radicals. Recent thermodynamic tables use enthalpies of formation of HO at 0 K of 39.0 ($\pm$2.1) kJ mol^{-1},[25,26] 38.39 ($\pm$1.21) kJ mol^{-1},[24] 39.11 ($\pm$0.21) kJ mol^{-1},[104] all data being based on spectroscopic measurements before 1970. Obviously, improved measurements, e.g., of the dissociation energy of HO are urgently required to improve the situation. Selecting the value of 39.11 kJ mol^{-1}, the enthalpy of reaction (1.1) is $\Delta H_0^o = +69.87$ kJ mol^{-1}. The uncertainty in $\Delta H_{f,0}^o$(HO) leads to uncertainties in K_{eq}. Using $\Delta H_{f,0}^o(\mathrm{HO})=39.11$ kJ mol^{-1},[104] e.g., one has $K_{eq}=3.79\times10^{-3}$ at 1000 K and $K_{eq}=0.819$ at 3000 K, while $\Delta H_{f,0}^o(\mathrm{HO})=38.39$ kJ mol^{-1} leads to[24] $K_{eq}=4.16\times10^{-3}$ at 1000 K and $K_{eq}=0.932$ at 3000 K. An uncertainty of $\Delta H_{f,0}^o$(HO) of $\pm$2.1 kJ mol^{-1} [25,26] correspondingly would result in uncertainties of K_{eq}, for the considered temperatures, in the 20%–30% range which is just the considered uncertainty of the rate measurements. The comparison of the measured k_1 and k_2 thus is limited by the uncertainty of K_{eq}. Selecting $\Delta H_{f,0}^o(\mathrm{HO})=39.11$ kJ mol^{-1}, we calculate

$$K_{eq}=17.0\times(T/1000\,\mathrm{K})^{-0.213}\exp(-8404\,\mathrm{K}/T), \tag{6.4}$$

over the range 1000–5000 K. Using this K_{eq}, we convert selected measurements of k_1 into k_2 and include the data in Fig. 17. The expressions from Refs. 9 and 11 in this case fit better to the present calculations. However, increasing $\Delta H_{f,0}^o$(HO) by 2 kJ mol^{-1} [essentially corresponding to a change from 8404 K to 8645 K in Eq. (6.2)] would lead to better agreement with the lower values of k_2 from Refs. 12, 13, 16, 17. The dilemma thus cannot be solved, before improved measurements of $\Delta H_{f,0}^o$(HO) or of k_1 are available.

Apart from these ''minor'' uncertainties in the comparison between experiments and calculations, the general agreement appears very satisfactory.

VII. CONCLUSIONS

The comparison between experimental data for k_1 and k_2 on the one hand and the present theoretical results on the other hand suggests that our treatment, both on the side of the *ab initio* potential and of the theoretical characterization of the dynamics, essentially is realistic. Our treatment describes the transition from a completely capture controlled process (1.2) [corresponding to complete exit control of reaction (1.1)] at low temperatures to a complex-forming bimolecular process with statistical competition between forward- and backward-dissociation of the HO_2^* adduct at high temperatures. This competition is a strong function of energy E and angular momentum J such that E- and J-specific unimolecular rate theory has to be employed. There is neither evidence for non-statistical effects nor for a contribution of excited electronic states of HO_2. *Ab initio* calculations of the potential on the highest possible level are required. The statistical SACM/CT approach apparently provides an adequate description of the dynamics. Nevertheless, our earlier simplified construction of the potential, combined with a simplified version of SACM,[50] already provided a surprisingly quantitative picture. In order to improve the relevance of a comparison of measured and calculated values of k_1, the enthalpy of formation of HO radicals has to be established with a better reliability. The present calculations can also be extended[105] to determine $H+O_2$ scattering cross sections. Comparisons with the new measurements from Ref. 40 are underway.

ACKNOWLEDGMENTS

Financial support of this work by the Deutsche Forschungsgemeinschaft (SFB 357 ''Molekulare Mechanismen unimolekularer Prozesse'') is gratefully acknowledged. L.B.H. is supported by the U.S. Department of Energy, Office of Basic Energy, Sciences, Division of Chemical Sciences, under Contract No. W-31-109-ENG-38.

APPENDIX: ADIABATIC CHANNEL MAXIMA

Adiabatic channel maxima are given in the form $E_0(l) - E_{\rm rot}(j) \approx E_0(l=0) + al^2 + bl^4$ with $E_{\rm rot}(j)$ = rotational energy of free HO (energies in $\rm cm^{-1}$, $k_{\rm cap}$ in $10^{-10}\,\rm cm^3\,molecule^{-1}\,s^{-1}$ for individual channels).

1. Closed shell treatment with structureless O+HO

$j=0$, $m=0$: adiabatic zero point barrier at $r=8.27$ Å; $E_0(l=0)=4.20$, $a=0.0317$, $b=0.143\times10^{-4}$; $k_{\rm cap} = 9.05\exp(19.2\,{\rm K}/T)\{1\text{-erf}[(25.3\,{\rm K}/T)^{1/2}]\}$.

$j=1$, $m=0$: adiabatic zero point barrier at $r=5.64$ Å; $E_0(l=0)=41.7$, $a=0.0641$, $b=0.160\times10^{-4}$; $k_{\rm cap} = 8.55\exp(32.2\,{\rm K}/T)\{1\text{-erf}[(92.2\,{\rm K}/T)^{1/2}]\}$.

$j=1$, $|m|=1$: adiabatic zero point barrier at $r=6.51$ Å; $E_0(l=0)=8.03$, $a=0.050$, $b=0.212\times10^{-4}$; $k_{\rm cap} = 7.44\exp(31.2\,{\rm K}/T)\{1\text{-erf}[(42.7\,{\rm K}/T)^{1/2}]\}$.

2. Open shell treatment with HO($^2\Pi_{3/2}$) + structureless O

The sign of the projection of the angular momentum on the intermolecular axis (quantum number m) corresponds to that of the projection of the electronic momentum of HO.

$j=3/2$, $m=1/2$: adiabatic zero point barrier at 7.77 Å; $E_0(l=0)=0.809$, $a=0.0377$, $b=0.332\times10^{-4}$; $k_{\rm cap} = 5.94\exp(14.2\,{\rm K}/T)\{1\text{-erf}[(15.4\,{\rm k}/T)^{1/2}]\}$.

$j=3/2$, $m=-1/2$: adiabatic zero point barrier at 5.24 Å; $E_0(l=0)=28.6$, $a=0.075$, $b=0.136\times10^{-4}$; $k_{\rm cap} = 9.29\exp(108\,{\rm K}/T)\{1\text{-erf}[(149\,{\rm K}/T)^{1/2}]\}$.

$j=3/2$, $m=3/2$: no adiabatic zero point barrier; $E_0(l=0)=0$, $a=0.314\times10^{-4}$, $b=0.432\times10^{-4}$; $k_{\rm cap}\approx5.21$.

$j=3/2$, $m=-3/2$: adiabatic zero point barrier at 4.75 Å; $E_0(l)=87.1$, $a=0.0904$, $b=0.134\times10^{-4}$; $k_{\rm cap} = 9.34\exp(93.7\,{\rm K}/T)\{1\text{-erf}[(219\,{\rm K}/T)^{1/2}]\}$.

[1] J. A. Miller, *26th Symposium (International) on Combustion* (The Combustion Institute, Pittsburgh, 1996), p. 461.
[2] I. W. M. Smith (private communication, April 2000).
[3] M. J. Howard and I. W. M. Smith, J. Chem. Soc., Faraday Trans. 2 **77**, 997 (1981).
[4] R. S. Lewis and R. T. Watson, J. Phys. Chem. **84**, 3495 (1980).
[5] W. H. Brune, J. J. Schwab, and J. A. Anderson, J. Phys. Chem. **87**, 4503 (1983).
[6] I. W. M. Smith and D. W. A. Stewart, J. Chem. Soc., Faraday Trans. **90**, 3221 (1994).
[7] K. H. Eberius, K. Hoyermann, and H. Gg. Wagner, *13th Symposium (International) on Combustion* (The Combustion Institute, Pittsburgh, 1971), p. 713.
[8] G. L. Schott, Combust. Flame **21**, 357 (1973).
[9] P. Frank and Th. Just, Ber. Bunsenges. Phys. Chem. **89**, 181 (1985).
[10] N. Fujii and K. S. Shin, Chem. Phys. Lett. **151**, 461 (1988).
[11] N. Fujii, T. Sato, H. Miyama, K. S. Shin, and W. C. Gardiner, *17th International Symposium on Shock Waves and Shock Tubes*, edited by Y. W. Kim (American Institute of Physics, New York, 1988), p. 456.
[12] A. N. Pirraglia, J. V. Michael, J. W. Sutherland, and R. B. Klemm, J. Phys. Chem. **93**, 282 (1989).
[13] D. A. Masten, R. K. Hanson, and C. T. Bowman, J. Phys. Chem. **94**, 7119 (1990).
[14] J. Vandooren, F. Neslon da Cruz, and P. J. Van Tiggelen, *22nd Symposium (International) on Combustion* (The Combustion Institute, Pittsburgh, 1988), p. 1587.
[15] T. Yuan, C. Wang, C.-L. Yu, M. Frenklach, and M. J. Rabinowitz, J. Phys. Chem. **95**, 1258 (1991).
[16] K. S. Shin and J. V. Michael, J. Chem. Phys. **95**, 262 (1991).
[17] H. Du and J. P. Hessler, J. Chem. Phys. **96**, 1077 (1992).
[18] J. V. Michael, Prog. Energy Combust. Sci. **18**, 327 (1992).
[19] C.-L. Yu, M. Frenklach, D. A. Masten, R. K. Hanson, and C. T. Bowman, J. Phys. Chem. **98**, 4770 (1994).
[20] H. Yang, W. C. Gardiner, K. S. Shin, and N. Fujii, Chem. Phys. Lett. **231**, 449 (1994).
[21] D. L. Baulch, D. D. Drysdale, D. G. Horne, and A. C. Lloyd, *Evaluated Kinetic Data for High Temperature Reactions* (Butterworths, London, 1972), Vol. 1; N. Cohen and K. R. Westberg, J. Phys. Chem. Ref. Data **12**, 531 (1983); J. Warnatz, in *Combustion Chemistry*, edited by W. C. Gardiner (Springer-Verlag, New York, 1984), p. 197.
[22] D. L. Baulch, C. J. Cobos, R. A. Cox, C. Esser, P. Frank, Th. Just, J. A. Kerr, M. J. Pilling, J. Troe, R. W. Walker, and J. Warnatz, J. Phys. Chem. Ref. Data **21**, 411 (1992).
[23] D. L. Baulch, C. J. Cobos, R. A. Cox, P. Frank, G. Hayman, Th. Just, J. A. Kerr, T. Murrells, M. J. Pilling, J. Troe, R. W. Walker, and J. Warnatz, J. Phys. Chem. Ref. Data **23**, 847 (1994).
[24] *NIST-JANAF Thermodynamical Tables*, edited by M. W. Chase, J. Phys. Chem. Ref. Data, Monograph No. 9 (1998).
[25] J. A. Kerr and D. W. Stocker, in *CRC Handbook of Chemistry of Physics*, 80th ed., edited by D. R. Lide (CRC Press, Boca Raton, 1999).
[26] D. Atkinson, D. L. Baulch, R. F. Hampson, J. A. Kerr, M. J. Rossi, and J. Troe, J. Phys. Chem. Ref. Data **29**, 167 (2000).

[27] H. Teitelbaum and A. Lifshitz, Phys. Chem. Chem. Phys. **2**, 687 (2000).
[28] S. O. Ryu, S. W. Hwang, and M. J. Rabinowitz, J. Phys. Chem. **99**, 13984 (1995).
[29] C. J. Cobos, H. Hippler, and J. Troe, J. Phys. Chem. **89**, 342 (1985).
[30] K. Kleinermanns and J. Wolfrum, J. Chem. Phys. **80**, 1446 (1984).
[31] A. Jacobs, F. M. Schuler, H. R. Volpp, M. Wahl, and J. Wolfrum, Ber. Bunsenges. Phys. Chem. **94**, 1390 (1990).
[32] K. Kleinermanns, E. Linnebach, and M. Pohl, J. Chem. Phys. **91**, 2181 (1989).
[33] K. Kessler and K. Kleinermanns, J. Chem. Phys. **97**, 374 (1992).
[34] A. Jacobs, H. R. Volpp, and J. Wolfrum, Chem. Phys. Lett. **177**, 200 (1991); **180**, 613 (1991).
[35] S. Sieger, V. Sick, H. R. Volpp, and J. Wolfrum, Isr. J. Chem. **34**, 5 (1994).
[36] M. J. Bronikowski, R. Zhang, D. J. Rakestraw, and R. N. Zare, Chem. Phys. Lett. **156**, 7 (1989); H. G. Rubahn, W. J. van der Zande, R. Zhang, M. Bronikowski, and R. N. Zare, *ibid.* **186**, 154 (1991).
[37] H. L. Kim, M. A. Wickramaaratchi, X. S. Zheng, and G. E. Hall, J. Phys. Chem. **101**, 2033 (1994).
[38] R. A. Fei, X. S. Zheng, and G. E. Hall, J. Phys. Chem. A **101**, 2541 (1997).
[39] K. Honma, J. Chem. Phys. **102**, 7856 (1995).
[40] C. Kappel, H. R. Volpp, and J. Wolfrum (private communication, April 2000).
[41] C. F. Melius and R. J. Blint, Chem. Phys. Lett. **64**, 183 (1979).
[42] M. R. Pastrana, L. A. M. Quintales, J. Brandao, and A. J. C. Varandas, J. Phys. Chem. **94**, 8073 (1990), and earlier references.
[43] B. Kendrick and R. T Pack, J. Chem. Phys. **102**, 1994 (1995).
[44] L. B. Harding, J. Troe, and V. G. Ushakov, Phys. Chem. Chem. Phys. **2**, 631 (2000).
[45] S. P. Walch, C. M. Rohlfing, C. F. Melius, and C. W. Bauschlicher, J. Chem. Phys. **88**, 6273 (1988); **90**, 7613 (1989).
[46] S. P. Walch and C. M. Rohlfing, J. Chem. Phys. **91**, 2373 (1989).
[47] S. P. Walch and R. J. Duchovic, J. Chem. Phys. **94**, 7068 (1991).
[48] C.-Y. Yang and S. J. Klippenstein, J. Chem. Phys. **103**, 7287 (1995).
[49] M. M. Graff and A. F. Wagner, J. Chem. Phys. **92**, 2423 (1990).
[50] J. Troe, *22nd Symposium (International) on Combustion* (The Combustion Institute, Pittsburgh, 1988), p. 843.
[51] J. Troe, J. Phys. Chem. **90**, 3485 (1986); Ber. Bunsenges. Phys. Chem. **94**, 1183 (1990).
[52] G. J. Vazquez, S. D. Peyerimhoff, and R. J. Buenker, Chem. Phys. **99**, 239 (1985).
[53] D. C. Clary and H.-J. Werner, Chem. Phys. Lett. **112**, 346 (1984).
[54] J. A. Miller, J. Chem. Phys. **84**, 6170 (1986); J. A. Miller and B. C. Garrett, Int. J. Chem. Kinet. **29**, 275 (1997).
[55] L. A. M. Quintales, A. J. C. Varandas, and J. M. Alvarino, J. Phys. Chem. **92**, 4552 (1988).
[56] A. J. C. Varandas, J. Chem. Phys. **99**, 1076 (1993); Chem. Phys. Lett. **225**, 18 (1994); **235**, 111 (1995).
[57] K. Kleinermanns and R. Schinke, J. Chem. Phys. **80**, 1440 (1984).
[58] G. Nyman, Chem. Phys. **173**, 154 (1993).
[59] A. J. C. Varandas, Mol. Phys. **186**, 1159 (1995).
[60] V. Klimo, M. Bittererova, S. Biskupic, and J. Urban, Chem. Phys. **173**, 367 (1993).
[61] A. D. Isacson and D. G. Truhlar, J. Chem. Phys. **76**, 1380 (1982).
[62] K. Song and W. J. Chesnavich, J. Chem. Phys. **91**, 4664 (1989); **93**, 5751 (1990).
[63] S. N. Rai and D. G. Truhlar, J. Chem. Phys. **79**, 6046 (1983).
[64] R. J. Duchovic and J. D. Pettigrew, J. Phys. Chem. **98**, 10794 (1994).
[65] J. Davidson and G. Nyman, Chem. Phys. **125**, 171 (1988); J. Chem. Phys. **92**, 2407 (1990); **92**, 2415 (1990).
[66] R. T Pack, E. A. Butcher, and G. A. Parker, J. Chem. Phys. **99**, 9310 (1993); **102**, 5998 (1995).
[67] C. Leforestier and W. H. Miller, J. Chem. Phys. **100**, 733 (1994).
[68] D. H. Zhang and J. Z. H. Zhang, J. Chem. Phys. **101**, 3671 (1994).
[69] A. J. Dobbyn, M. Stumpf, H.-M. Keller, W. L. Hase, and R. Schinke, J. Chem. Phys. **102**, 5867 (1995); **103**, 9947 (1995); **104**, 8357 (1996).
[70] R. Schinke, Ber. Bunsenges. Phys. Chem. **102**, 593 (1998).
[71] E. M. Goldfield and S. K. Gray, Chem. Phys. Lett. **276**, 1961 (1997).
[72] A. J. H. M. Meijer and E. M. Goldfield, J. Chem. Phys. **110**, 870 (1999).
[73] A. I. Maergoiz, E. E. Nikitin, J. Troe, and V. G. Ushakov, J. Chem. Phys. **108**, 5265 (1998); **108**, 9987 (1998).
[74] B. Abel, J. Troe, and V. G. Ushakov, J. Chem. Phys. (to be published).
[75] B. Abel, A. I. Maergoiz, and J. Troe, J. Chem. Phys. (to be published).
[76] W. H. Miller, W. L. Hase, and C. L. Darling, J. Chem. Phys. **91**, 2863 (1989); J. M. Bowman, B. Gazdy, and Q. Sun, *ibid.* **91**, 2859 (1989).
[77] A. I. Maergoiz, E. E. Nikitin, and J. Troe, Z. Phys. D: At., Mol. Clusters **36**, 339 (1996); J. Troe, Ber. Bunsenges. Phys. Chem. **99**, 341 (1995).
[78] J. Troe, *28th Symposium (International) on Combustion* (The Combustion Institute, Pittsburgh, 2000).
[79] J. Troe, Chem. Phys. **190**, 381 (1995).
[80] T. H. Dunning, J. Chem. Phys. **90**, 1007 (1989).
[81] R. A. Kendall, T. H. Dunning, and R. H. Harrison, J. Chem. Phys. **96**, 6796 (1992).
[82] D. E. Woon and T. H. Dunning, J. Chem. Phys. **98**, 1358 (1993).
[83] S. R. Langhoff and E. R. Davidson, Int. J. Quantum Chem. **8**, 61 (1974); D. W. Silver and E. R. Davidson, Chem. Phys. Lett. **52**, 403 (1978).
[84] MOLPRO is a package of *ab initio* programs written by H.-J. Werner and P. J. Knowles with contributions from J. Almlof, R. D. Amos, A. Berning *et al.*
[85] H.-J. Werner and P. J. Knowles, J. Chem. Phys. **82**, 5053 (1985); P. J. Knowles and H.-J. Werner, Chem. Phys. Lett. **115**, 259 (1985); H.-J. Werner and P. J. Knowles, J. Chem. Phys. **89**, 5803 (1988); P. J. Knowles and H.-J. Werner, Chem. Phys. Lett. **145**, 514 (1988).
[86] L. B. Harding, Ber. Bunsenges. Phys. Chem. **101**, 363 (1997).
[87] M. Litorja and B. Ruscic, J. Electron Spectrosc. Relat. Phenom. **97**, 131 (1998).
[88] K. J. Holstein, E. H. Fink, J. Wildt, R. Winter, and F. Zabel, J. Phys. Chem. **87**, 3943 (1983); S. T. Lunt, G. Marston, and R. P. Wayne, J. Chem. Soc., Faraday Trans. 2 **84**, 899 (1988).
[89] J. M. Oakes, L. B. Harding, and G. Barney Ellison, J. Chem. Phys. **83**, 5400 (1985).
[90] L. B. Harding, H. Stark, J. Troe, and V. G. Ushakov, Phys. Chem. Chem. Phys. **1**, 63 (1999).
[91] J. Troe, J. Chem. Soc., Faraday Trans. **90**, 2303 (1994).
[92] J. Troe, J. Chem. Phys. **79**, 6017 (1983); **105**, 6249 (1996).
[93] P. R. Bunker, I. P. Hamilton, and P. Jensen, J. Mol. Spectrosc. **155**, 44 (1992).
[94] J. Troe, Chem. Phys. **190**, 381 (1995).
[95] D. Reignier and T. Stoecklin, Chem. Phys. Lett. **303**, 576 (1999).
[96] T. Stoecklin, Chem. Phys. Lett. **237**, 516 (1995).
[97] T. Stoecklin, C. E. Dateo, and D. C. Clary, J. Chem. Soc., Faraday Trans. **87**, 1667 (1991).
[98] J. H. Black and P. L. Smith, Astrophys. J. **277**, 562 (1984); E. Roueff and D. Williams (work in progress).
[99] I. W. M. Smith (private communication, April 2000).
[100] D. L. Baulch, R. A. Cox, R. F. Hampson, J. A. Kerr, J. Troe, and R. T. Watson, J. Phys. Chem. Ref. Data **9**, 295 (1980).
[101] A. I. Maergoiz, E. E. Nikitin, and J. Troe, J. Chem. Phys. **103**, 2083 (1995).
[102] W. R. Gentry and C. F. Giese, J. Chem. Phys. **67**, 2355 (1977).
[103] P. Frank and Th. Just (private communication, May 2000).
[104] *Thermodynamic Properties of Individual Substances*, 4th ed., edited by L. V. Gurvich, I. V. Veyts, and C. B. Alcock (Hemisphere, Taylor & Francis, New York, 1989).
[105] M. Quack and J. Troe, Ber. Bunsenges. Phys. Chem. **79**, 170 (1975).